Research Article

Abdalla M. Darwish*, Sergey S. Sarkisov*, Brandon Graycol, Anja Hribljan, Darayas N. Patel, Alex Fedoseyev, David Hui, Paolo Mele, Giovanna Latronico, Kyu Cho, Anit Giri, and Brent Koplitz

Polymer nanocomposite for protecting photovoltaic cells from solar ultraviolet in space

https://doi.org/10.1515/ntrev-2024-0013
received May 17, 2023; accepted March 19, 2024

Abstract: Polymer nanocomposite coatings of solar photovoltaic cells that absorb solar ultraviolet (UV) radiation and convert it into visible and near-infrared (NIR) light can increase the operational lifetime and the energy efficiency of the cells. We report a polymer nanocomposite spectrum converting layer (SCL) made of colorless polyimide CORIN impregnated with the nanoparticles (NPs) of fluoride $NaYF_4$ doped with three-valent ions of Europium at a molar concentration of 60%. The NPs were the nanocrystals (179 ± 35 nm in size) in thermally stable hexagonal beta-phase. The visible-NIR photoluminescence quantum yield of the nano-powder was ~69%. The SCLs were applied using the open-air multi-beam multi-target pulsed laser deposition method to silicon heterojunction (SHJ), copper-indium-gallium-selenide (CIGS), and inverted metamorphic multijunction (IMM) solar cells. The cells were exposed to UV radiation from a 365 nm light emitting diode. The *I-V* characteristics of the cells were measured with a solar simulator using AM0 filter. The proposed SCLs improved the UV stability of all three types of the cells: the power degradation of SHJs and IMMs cells was stopped or slightly reversed and the degradation rate of CIGSs decreased by ~25%. The proposed SCLs have great commercial potential, especially for applications to spare power.

Keywords: rare earth doped compounds, silicon heterojunction solar cell, copper-indium-gallium-selenide solar cell, inverted metamorphic multijunction solar cell, solar power, renewable energy, pulsed laser deposition, space vehicles

* **Corresponding author: Abdalla M. Darwish,** Physics and Pre-Engineering Department, Dillard University, New Orlean, sLA 70122, United States of America, e-mail: adarwish@dillard.edu
* **Corresponding author: Sergey S. Sarkisov,** SSS optical Technologies, LLC, Huntsville, AL 35816, United States of America, e-mail: mazillo123@yahoo.com
Brandon Graycol, Anja Hribljan: Physics and Pre-Engineering Department, Dillard University, New Orleans, LA 70122, United States of America
Darayas N. Patel: Department of Mathematics and Computer Science, Oakwood University, Huntsville, AL 35896, United States of America
Alex Fedoseyev: Solestial, Inc., Tempe, AZ 85284, United States of America
Dav id Hui: Department of Mechanical Engineering, University of New Orleans, New Orleans, **LA** 70148, United States of America
Paolo Mele: College of Engineering, Shibaura Institute of Technology, Saitama, 337-8570, Japan
Giovanna Latronico: College of Engineering, Shibaura Institute of Technology, Saitama, 337-8570, Japan; International Research Fellow of Japan Society for the Promotion of Science USPS), Saitama, 337-8570, Japan
Kyu Cho, **Anit Giri:** Army Research Laboratory, Weapons & Materials Research Directorate, Aberdeen Proving Ground, MD 21005, United States of America
Brent Koplitz: Chemistry Department, Tulane University, New Orleans, LA 70118, United States of America

Abbreviations

AM	air mass
AO	atomic oxygen
BOL	beginning-of-life
CTGS	copper-indium-gallium-selenide
DLS	dynamic light scattering
EDTA	Narethylenediaminetetraacetic acid
EOL	end-of-life
ESH	equivalent sun hours
GPIB-USB	general purpose interface bus-universal serial bus
IMM	inverted metamorphic multijunction
IPCE	incident photon to charge carrier efficiency
I-V	current-voltage
JCPDS	joint committee on powder diffraction standards
LED	light emitting diode
MBMT-PLD	multi-beam multi-target pulsed laser deposition
Nd:YAG	neodymium doped yttrium aluminum garnet
NP	nanoparticle
NIR	near-infrared
OS	oligomeric silsesquioxane

PL	photoluminescence
PLD	pulsed laser deposition
PLQY	photoluminescence quantum yield
PV	photovoltaic
RE	rare-earth
SCL	spectrum converting layer
SEM	scanning electron microscopy
lN	ultraviolet
VIS	visible
XRD	X-ray diffraction

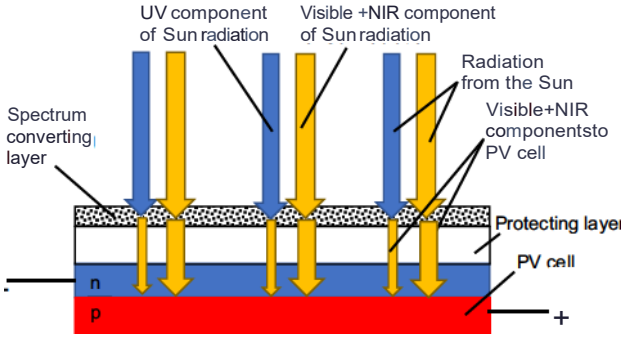

Figure 1: Sketch illustrating the usage of an SCL on the top of a solar PV cell. There is also solar UV, visible, and NIR radiation reflected from the SCL and the down-shifted visible and NIR radiation emitted by the SCL upwards that is not shown in the sketch.

1 Introduction

Significant efforts have been put toward the development of polymer coatings protectingphotovoltaic (PV) solar cells against harmful ultraviolet (UV) spectral components of solar radiation reducing operational lifetime (1- 5). The advantages of a polymer protecting layer over previously used semi-flexible cover glass are flexibility and light weight. This is critical for space applications with ultra-compact solar array deployment systems such as NASA's Lightweight Integr ated Solar Array and AnTenna, slip wrapping concept by Caltech, and R3D2 antenna deployment system by MMA Design developed for small spacecraft (6). While protecting a solar cell, the polymer overcoat itself is subject to degradation under exposure to solar lN. This degradation revea1s as darkening, yellowing. or sublimation (6). Besides, the energy of lN radiation just gets wasted in the polymer layer without producing electricity. In this study, we describe our efforts to make polymer nanocomposite layers that convert lN into visible and near-infrared (NIR) light that can be used by solar PV cells for producing extra electricity. We call such coatings the spectrum converting layers (SCLs). The configuration of a PV cell coated with an SCLis schematically presented in Figure1. The SCL made of a polymer nanocomposite embedded with nanoparticles (NPs) is deposited ona protective (optically transparen t) layer on the top of the PV cell. Both lN and visible-NIR spectral components of sun radiation reach the SCL. lN component is absorbed by the NPs and spectrally converted into visible-NIR radiation though the mechanism of downshifting. The visibfo-NIR radiation produced by the spectrum conversion along with the major visible-NIR components pass to the PV cell and generate extra electricity. On their passage through the SCL and the protecting layer, the major and extra visible-NIR radiation might have losses due to reflection, absorption, and scattering. Accordingly, the major yellow arrows below the SCL are shown slightly thinner. Protecting transparent layer can be absent. The SCL is expected to shield itself and the protecting layer and PV cell covered by it from solar lN radiation thus increasing operational lifetime. It must also improve photoelectric energy conversion efficiency. In this work, for the first time to our knowledge, we demonstrated that the proposed SCLimproved thelN stability of threetypes of PV cells suitable for space power.

In Section 2 we describe the mechanism of spectrum conversion, the selection, and synthesis of the materi als, making SCLs, and building the experimental setup for testing SCL prototypes. Section 3 includes the results and discussion of the experimental characterization of the performance of the SCL prototypes integrated with typical solar cells, including the candidates for space solar arrays followed by the conclusion in Section **4.**

2 Materials and methods

2.1 Solar spectrum converting NPs

Among possible candidates for spectral conversion, weselected the NPs made of fluoride $NaYF_4$ doped with three-valent ions of rare-earth (RE) element Europium. $NaYF_4$ is a suitable host for RE ions due its low phonon energy (- 300 cm^{-1}) that makes multi-phonon assisted nonradiative relaxation of the excited ions weak f7). Superior performance of Eu^{3+} as an efficient spectrum converter in various inorganic matrices has been reported in the literature (8-18).

The powders of Eu-doped $NaYF_4$ compound were synthesized using the economic wet process, which in its essence is co-precipitation in the presence of Narethylenediaminetetraacetic acid (EDTA). In a typical procedure, 21g NaF (0.05 mol) was dissolved in 60mL of deionized water. Another solution

was prepared by mixing *a* x 16mL of 02-moVL aqueous solution of YCl_3 and *b* x 16 mL of 02-moVL solution of $EuCl_3$ and 20mL of 02-moVL EDTA aqueous stock solution to form the metal-EDTA complex (*a* + *b* = 1). All the chemicals were acquired from Millipore-Sigma. The complex solution was injected in the NaF solution quickly, and the mixture was stirred vigorously for 1h at room temperature. After stirring, the mixture was allowed to stay overnight for the precipitate to settle. The precipitate was collected and washed several times with distilled water and anhydrous ethanol. In the second stage of the process, the precipitate was dried under vacuum to remove any traces of water. The resulting micrercrystalline powder had a doping rate according to formula NaYJ 4: Eur For instanc,ethe 10% molar concentration of Eu corresponded to *a* = 0.9, *b* = 0.1 We synthesized the powders at various molar proportions between Y and Eu.

To investigate crystalline properties, we conducted the X-ray diffraction (XRD) spectroscopy of the obtained powders using a Bruker D2 Phaser X-ray diffractometer. The results are presented in Figure 2. Spectrum 1 corresponds to a portion of compound $NaY_{0}gF_4$: Eu5 intentionally heat-treated at 500°C for 1 h. All other spectra are of freshly made compounds without heat treatment. Spectrum 1 is like the one of hexagonal -phase of $NaYF_4$ (JCPDS No. 28-1192) that agrees with our earlier findings about heat treatment in the study by Patel *et aL* (19). Spectra 2 and 3 of unheated powders with molar concentrations 10 and 20% of Eu3+, respectively, are like the ones of cubic a-phase of $NaYF_4$ (JCPDS No. 77-2042). This is also in agreement with the study by Patel *et al.* (19]. There is a little shift of the diffraction peaks to the left due to a slight change in the lattice volume caused by the substitution of Yttrium ions in their sites by Europium ions. However, for a molar concentration of 40% of Eu^{3+}, spectrum 4 becomes a mixture of the a- and !3--ph ases, and for 60% of Eu^{3+}, spectrum 5 is like the one of hexagonal -phase of $NaEuF_4$ (JCPDS No. 49-1987) (20].

The synthesized compounds were reduced to nano-powders by ball-milling in water using a PQ-N04 Planetary Ball Mill from Across International. The nano-powders were dried and transferred to organic solvent digl.yme. The size distribution of the obtained NPs was measured using the Dynamic Light Scattering (DLS) method with a Zetasizer DLS instrument from Malvern Instruments. DLS scan of the size distribution of the NPs is presented in Figure 3. The size of the NPs (assuming their spherical shape) was determined as 179 ±35nm.

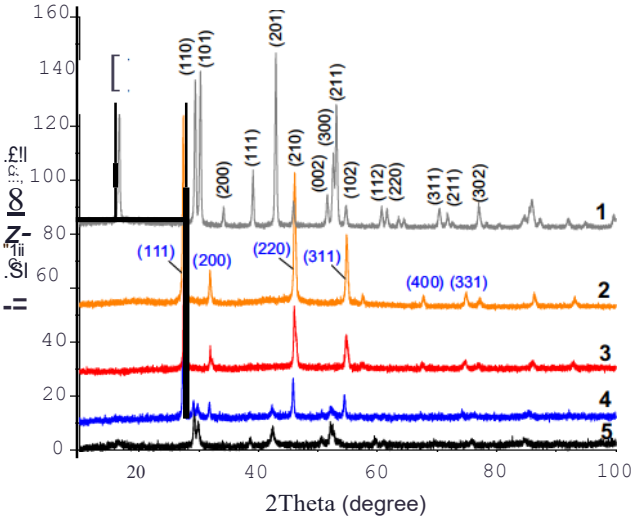

Figure 2: XRD spectra of NaYF4:Eu^{3} powders at different molar concentrations of Eu. Spectrum 1 corresponds to $NaY_{0.9}F_4$ Eu ; heat-treated at 500° (for 1h; Spectrum 2 - freshly made $NaY_{09}F_4$ EuJ; ; Spectrum 3 - freshly made $NaY_{0.}F_4$ Eu ; Spectrum 4 -freshly made $NaY_{06}F_4$ $Eu_{0.}l$•; Spectrum 5 - freshly made $NaY_{04}F_4$Eu- Numbers in parenthesis are triple-digit Miller indices. Spectrum 1 is like the spectrum of hexagonal 13-phase of NaYF4 OCPDS No. 28-1192); Spectrum 2 is like the spectrum of cubic a-phase of NaYF4 OCPDS No. 77-2042); Spectrum 5 is like the spectrum of hexagonal !3-phase of NaEuF4 OCPDS No. 49-1987) .

2.2 Optical properties of the spectrum converting compounds

The mechanism of spectrum conversion in Eu^{3+} is down-shifting as illustrated in the energy level diagram in Figure 4 (21.] After absorlling lN photons and making transitions shown in the left part of the diagram, excited Eu^{3} ions radiationlessly relax to lower energy levels and emit visible and NIR photons

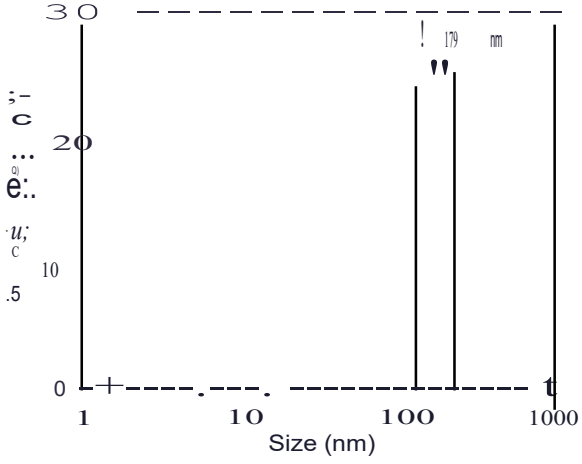

Figure 3: Size distribution of the NPs dispersed in diglyme. Concentration was -4 mg of solids per -3 ml liquids. The nanocolloid was filtered with a 1.0µm filter.

during the transition further down the energy ladder in the right half of the diagram. The samples for optical spectroscopy measurements were prepared by compressing the nano-powders into pellets using a 5-T hydraulic press. Figure 5 presents the diffuse reflectance spectrum of NaY_0,f 4:Eu 1 sample measured with a Shimadzu lN-2600-ISR-2600 Plus lN-VIS-NIR spectrophotometer with an integrating sphere (measurable spectral range was 190-1,400 nm). The inverted absorption peaks can be attributed to the transitions of Eu^{3+} ions to excited states: $^7F_0$ $^5D_3$ (362 nm), $^7F_0$ ^{5} (375 nm), $^7F_0$ ^5Gz (382 nm), $^7F_0$ $^5L_6$ (395 nm), ^7F (415 nm), $^7F_0$ ^5Dz (465 nm), $^7F_0$ ^5Di (526 nm), $^7F_1$ ^5Di (535 nm), and $^7F_1$ $^5n_0$ (590 nm) shown in the left, "Absorption" part of the energy level diagram in Figure 4. Photoluminescence (PL) spectroscopy of the nano-powders was conducted with a spectrometer AvaSpec-ULS4096CL-EVO with integrating sphere AvaSphere-30 from Avantes and a fiber-coupled lN light emitting diode (LED) M365FP1 from Thorlabs (365 nm emission peak, 11 nm bandwidth) as a source of lN excitation. This source was suitable for simulating lN-A solar spectrum. The powder of heat-treated compound Na_Y_0gF4: Eu ; did not exhibit noticeable PL. All the unheated powders demonstrated PL with the intensity increasing with the increase in the concentration of Eu^{3+}. Starting from fi0% molar concentration of Eu(NaY_0J' 4:Eu .the powders did not change their crystalline phase after heating at S00°C for several hours. They remained to be like hexagonal phase of NaEuF4. Correspondingly, heating did not bring the drop of PL intensity. This stability of PL under heating indicated that the SCL coated solar cells would operate steadily in space where the temperature exceeds +120°C (near earth or on the moon) or at higher temperatures (closer to the sun or near venus and mercury due to their surface heating).

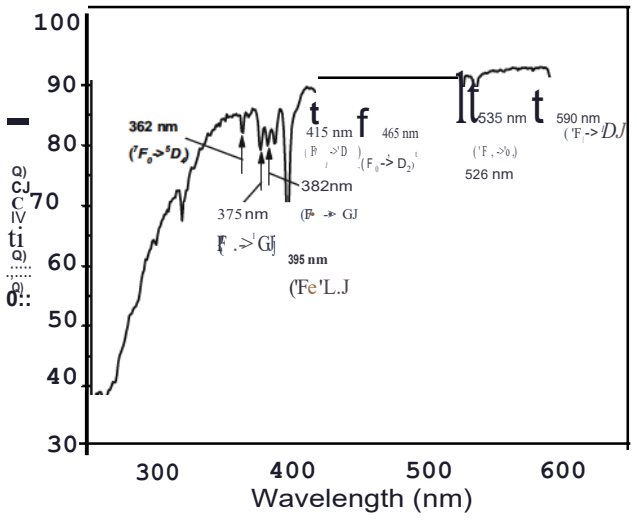

Figure 5: Diffuse reflectance spectrum of NaY_0_F4: Eui powder.

Figure 6 presents the PL spectrum of the NPs of NaY_0J' 4:Eugj, illuminated with the 365nm lN LED (its normalized emission spectrum is presented in the insert). The overall PL intensity and the intensity of individual peaks varied within no more than the 30% range from batch to batch of the synthesized NaY_0J',i:Eugj, powder. The plot in Figure 6 corresponds to the batch with the highest overall PL intensity that we used for making all the SCL samples in this study. PL peaks correspond to the transitions of the excited Eu^{3+} ions to the lower energy states in accordance with the right "Emission" part of the energy level diagram in Figure 4. Dominant spectral peaks (at 615 and 623 nm) were in

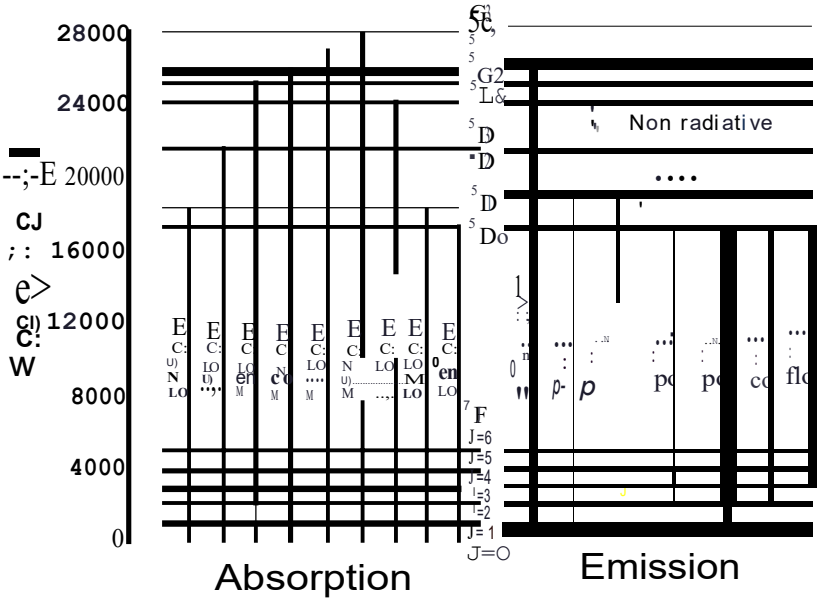

Figure 4: Energy level diagram of an Eu^{3+} ion (21].

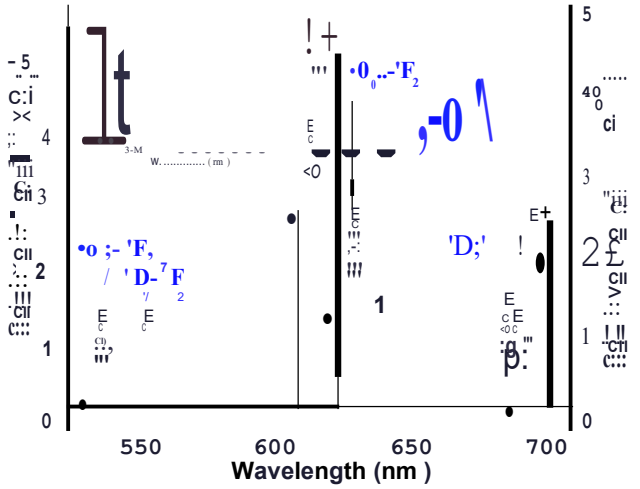

Figure6: PL spectrum of (1) $NaY_{0.4}F_4$: Eu powder sample and (2) the SCL over an SHJ cell illuminated by the 365nm UV LED M365FP1 (13.7mW/cm^2 irradiance). The left vertical axis corresponds to plot **1** and the right to plot 2. The relative PL intensities of both spectra were computed by dividing actual intensities by the peak intensity of the incident UV radiation. The insert presents the normalized spectrum of the incident radiation from the UV LED. The spectrum of the UV LED simulated the UV-A spectral component of sun radiation.

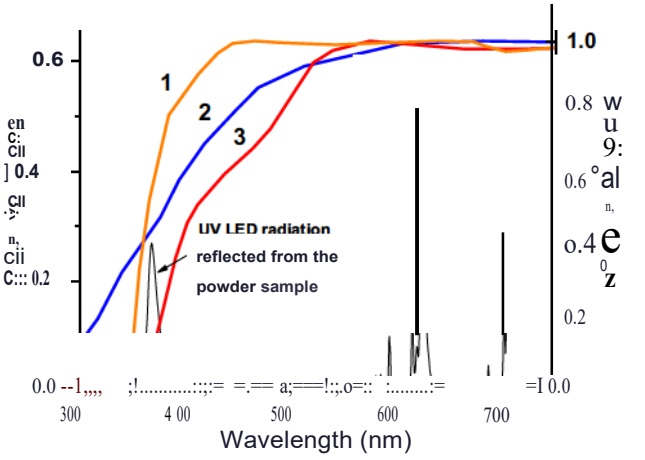

Figure 7: PL spectrum of $NaY_{0.4}F_4$: Eu powder in Figure 6 presented together with the spectral peak of the pumping UV LED radiation reflected from the powder sample. Also shown are the normalized IPCE spectra of (1) IMM [23], (2) SHJ [24], and (3) CIGS [25] solar cells used in this study.

the band corresponding to transition $^5D_0 \rightarrow {}^7F_2$. The maximum PL quantum yield (PLQY, the ratio of the number of visible-NIR photons to the number of exiting lN photons) of the nano-powder was estimated using the method described in the study by Zhydachevskyy *et al* (22) as --69%. Figure 7 shows the PL spectrum of the nanopowder (presented in Figure 6) together with the spectrum of the lN LED radiation reflected from the powder pellet together with the spectra of Incident photon to charge carrier efficiency (IPCE) of three types of PV cells used in this wmk The PL spectrum matched well with the IPCE spectra of the cells.

2.3 Polymer nanocomposite SCLs

For making SCLs, the NPs of Na_Y_0,iF_4: Eu5 were dispersed in polymer CORIN® XLS from Nexolve (1). It is a fluorinated colorless polyimide with durability to atomic oxygen (AO) and oxygen plasma. It was designed to be a light-weight substitute material for the cover glass used in space PV arrays in low earth orbit. Polyimide molecules (Figure 8) have tethered oligomeric silsesquioxane (OS) pendant groups providing AO durability (26,27). Figure 9 presents the typical optical transmittance spectra of the film of pure CORIN and SCL on a glass substrate measured with the Shimadzu spectrophotometer.SCL had ~20% less transmittance than CORIN in visible spectral region due to stronger haziness. Haziness resulted more likely from light scattering on the large-size particles in the nanocomposite SCL. The insert in Figure 9 shows the scanning electron microscope (SEM) image of the SCL with evenly distributed NPs of the size distributed according to Figure 3. However, few large-size (>200 nm) particles can also be seen in the image. While the CORIN-coated glass sample did not transmit short-wave radiation with a wavelength shorter than350 nm, the SCL-coated slide still transmitted radiation with a wavelength down to 300nm. This could be because of weaker reflectance of the short-wave radiation from the interface between the SCL and the glass.

SCLs were deposited on solar cells using the open-air multi-beam multi-target pulsed laser deposition method invented by D. Darwish (28-46). The advantages of the method are low consumption of the material, potentially high accuracy of the thickness of the deposited layer (unfortunatelynot implemented in this work), and precise control of the concentration of the constituents along and across the deposited layer. We used two variants of the method. The first variant included preparation of a nano-composite SCL compound by adding NPs to CORIN solution in diglyme at a proportion of approximately 0.53mg solids per mL liquids and intense stirring. An SCL was then deposited on a moving solar cell using the ejection in open air (with fl.owing argon) of the liquid composition with a pulsed laser beam (46). In the second var iant, SCLs were deposited on solar cells using the open-air (with fl.owing argon) two-beam two-target PLD (43,46). The first target was a pellet of a compressed spectrum converting nano-powder. The second target was a solution

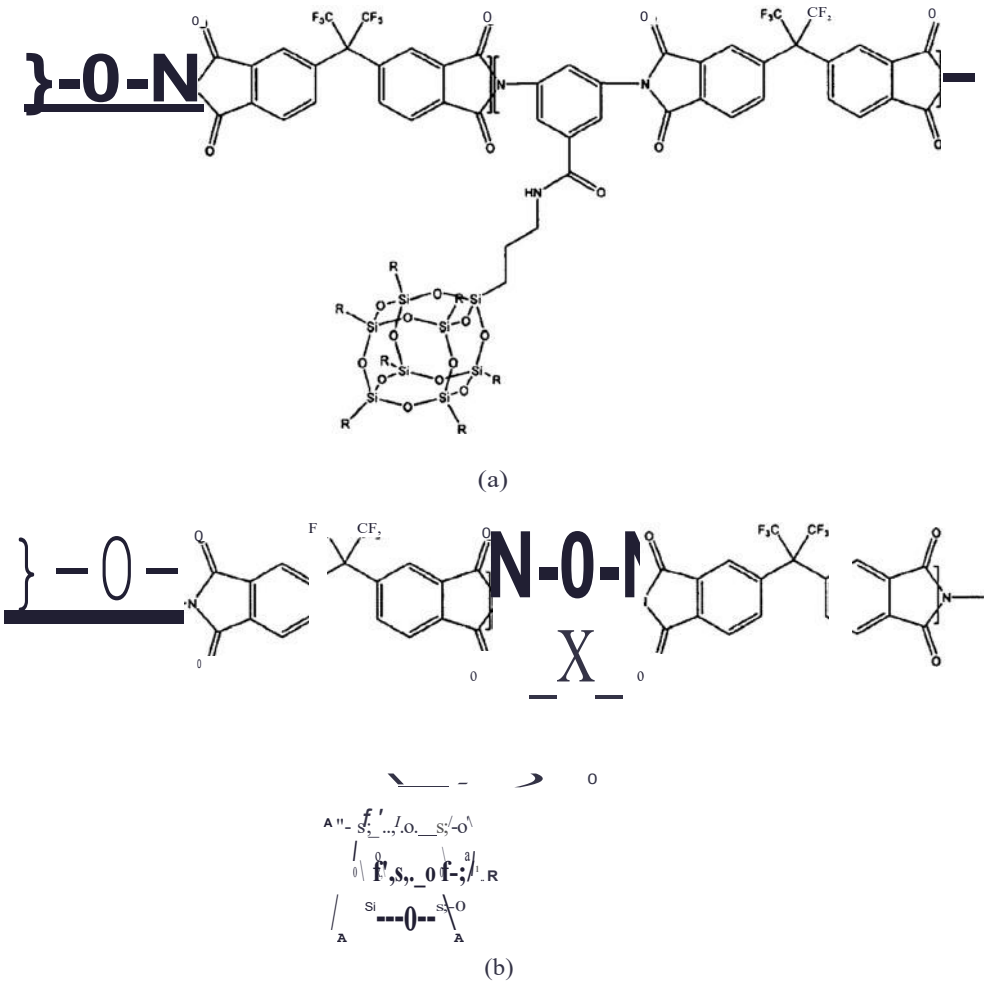

Figure8: Chemical formula of the chain link of CORIN polyimide with tethered OS pending unit connected wit h (a) an amide and (b) an ester.

of CORIN in diglyme. A1,064nm Q-switched Nd:YAG pulsed laser with 9-ns-longpulses, 0.4 J en er gy per pulse, and 10 pulses per second pulse rate was used as a source of laser pulses. After deposition, the polymer nanocomposite layers were heat-cured using a heat gun and overnight baking on a hot plate in ambient air at 80°C.

2.4 Experimental setup

Figure10 presents the schematic of the experimental setup for testing SCL pro to types integrated with PV cells . A solar simulator LCS-100 model 94011A-ES from MKS-Newport with a Xe-lamp and Air Mass **(AM)** 0 filter (simulating solar spectrum above the atmosphere) was used as a light source. The shutter of the simulator was controlled with a shutter contr oller 71445 from MKS-Newport . Theintensity of the light on the surface of a PV cellwas adjusted by changing elevation of the solar simulator over the cell The irradiance in "suns," the units equivalent to the sun irradiance on the ground (100 mW/cm^2), was measured with a calibrated reference PV cell and a calibrated meter model 91150 V from MKS-Newport.The measurement of *1- V* characteristics was conducted automatically under computer control using LabVIEW software developed for MKS-Newport *1- V* Test Station PVIV-1A (47). Voltage was automatically applied to the PV cell, and the flowing electric current was measured by a computer controlled Keithley 2400 Source and Measurement Unit. The unit was connected to the computer through GPIB-USB interface.

The uncoated and coated solar cells were exposed in vacuum to UV radiation from 50 to 100W LED arrays from Shenzhen Chanzon Technology Co., Ltd This radiation had a spectral band of -20 nm around the peak at 365 nm suitable to simulate UV-A component of solar UV spectrum in space. Exposure time was calibrated in the Equivalent solar hours (ESH).

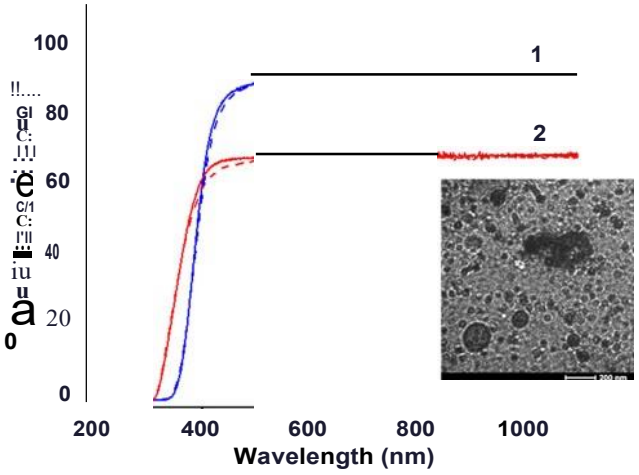

Figure 9: Typical optical transmittance spectrum of (1) the coating made of pure CORIN (thickness=15±6.4µm) and (2) SCL (thickness=17.1±5.9 µm) on a 158 µm thick microscope cover glass. Dashed lines show the transmittance after exposure to UV radiation in vacuum for 1,600 ESH. The insert is the high-resolution SEM image of the SCL coating taken with a JEOL SEM instrument. Dari< dots are the NPs.

3 Results and discussion

31 1 *1-V* characteristics of t he coated PV cells

For testing SCLs, we chose three types of solar cells: silicon heterojW1ction (SHJ) cells from Solestial (dimensions: 3.0 cm x 4.65 cm, ~14.0 cm^2 area and dimensions: 3.0cm x 5.2 cm, 15.6 cm^2 area), copper-indium-gallium-selenide (CIGS) flexible cells (dimensions: 4.75cm x 4.75cm, 17.77-cm^2 active area; according to the manufacturer, the cells are "truly bare" with no protective coating over the front conductors made of silver conductive paste), and epitaxial lift-off inverted metamorphic multijW1ction (IMM) flexible cells from MicroLlnk (dimensions: 3.0 cm x 6.6cm, 19.8 cm^2 area). Investigation of possible improvement in the PV energy conversion efficiency of PV cells and lN stability was conducted by comparing the *1-V* characteristics of the cells coated with SCLs against bare cells or the cells coated with pure CORIN. A total of five randomly picked SHJ, eight CIGS, and five IMM cells were used in the study. SHJ and IMM cells demonstrated no noticeable ageing for at least 8 months of storage in the lab conditions at room temperature. CIGS cells, according to manufacturer's recommendations, were stored in inert gas (argon) atmosphere at room temperature (to prevent degradation of silver front conductors) and did not show ageing for 6 months. The thicknesses of SHJ, CIGSand IMM cells were measured as 250± 2,68 ±3, and 30±2 µm, respectively. The thickness of CORIN/SCL coating on SHJ cells was not possible to measure precisely because the polymer penetrated inside the micro-pores on the surface made by etching to reduce optical reflectance. It was estimated to be between 6 and16 µm. The thicknesses of CORIN/SCL coatings of CIGS cells after curing were measured as 15.6 ± 8.1 µm; the CORIN/SCL on IMM thicknesses were measured as 61 ±3.2 µm. Despite being uneven, the coatings were optically smooth (roughness did not exceed ~02-0.3µm) since they demonstrated mirror-like reflection of incident light

The PL spectrum of the SCL excited by the 365 nm UV LED is presented in Figure 6 (curve 2). It fully replicated the

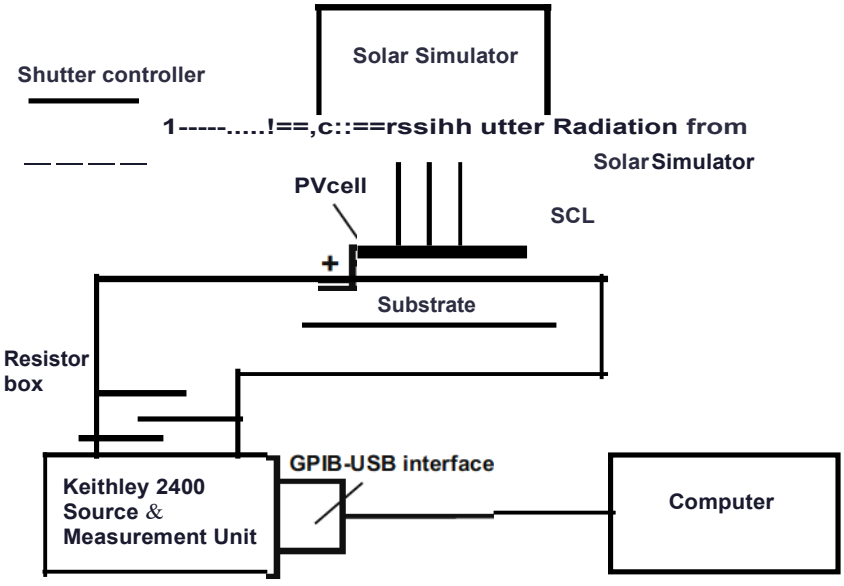

Figure 10: Schematic of the experimental setup for testing SQ prototypes deposited on ***PV*** cells.

PL spectrum of the Eu-doped nano-powder excited with the same source (Figure 6, curve 1). PLQY of the SCL was estimated as - 0.5%, much less than that of the n ano-powder. This was because the dispersion of the NPs in the solid polymer matrix at a concentration of - 26.5 mg/mL resulted in - 6.4 x 10^{19} cm ^{3} concentration of the photoluminescent spectrum downshifting Eu^{3+} ions while their concentration in the nano-powder was -1.3 x 10^{22} cm ^{3}, 203 times greater. Second, the incident UV radiation was partially absorbed in the CORIN polymer matrix of the SCL. We also inspected the spectra of the solar simulator radiation reflected from the SCL-coated PV cells in comparison with the spectra from CORIN-coated on es. Typical examples are presented in Figure 11 (SCL on an SHJ cell) and Figure 12 (SCL on an IMM cell). Zoom-in inserts in the figures show the difference between SCL-related and non-SCL spectra in the region 550- 650 nm whe re the PL peaks at 615 and 623nm attributedto the SCL are disce rnible. This extra visible/NIR PL radiation generated by the SCL joined the visible/NIR light from the solar simulator on its passage to the PV cell according to the concept illustra ted in Figure 1.

Graphs in Figure 13a and b present the *I- V* characteristics of the SHJ cells before and after coating with no exposure to UV radiation. For the sake of comparability of the *I- V* characteristics regardless of the actual area of the cells, instead of photoelectric current *I* current density *J* was used in all *I- V* plots. Figure 13a illustrates the case when two layers of CORIN were deposited and Figure 13b illustrates the case when one layer of CORIN and the SCL on the top as in the configuration in Figure 1 (bottom CORIN functioned as a protecting layer). In both cases the coatings brought the photogenerated current density down compared to the no-coating case, SCL brought it down more.

Figure 13cpresents the photograph of a bare SHJ cell at room illumination. The cell was cut from a 5-inch (127-mm) SHJ wafer. An SHJ wafer coated with one layer of CORIN and SCL on the top and illuminated with a 365-nm UV LED is shown in Figure 13d. Red PL was produced by the SCL.

The performance parameters extracted from the *I- V* characteristics in Figure13a and b (as described in the Application Note (48]) are presented in Table 1, the third and fourth columns, rows 2 through 5. Besides standard parameters, such as open circuit voltage V_{oc}, short circuit current I_{sc}, short circuit current density J_{sc}, maximum power P_{max}, and efficiency η, we also computed maximum power density PDmax = P_{max}/A, where A is the active cell area. This parameter was convenient in comparing PV power generated by different cells regardless of their actual area. As can be seen from Table 1 (the fourth column, rows 2 and 3), the 0.1% drop of η of the unexposed bare cell from 11.2 down to 11.1% brought by the double-layer CORIN coating was statistically insignificant: less than the maximal statistical spread of 1.0%. The SCL-caused 21% efficiency drop from 13.9 down to 11.8% was

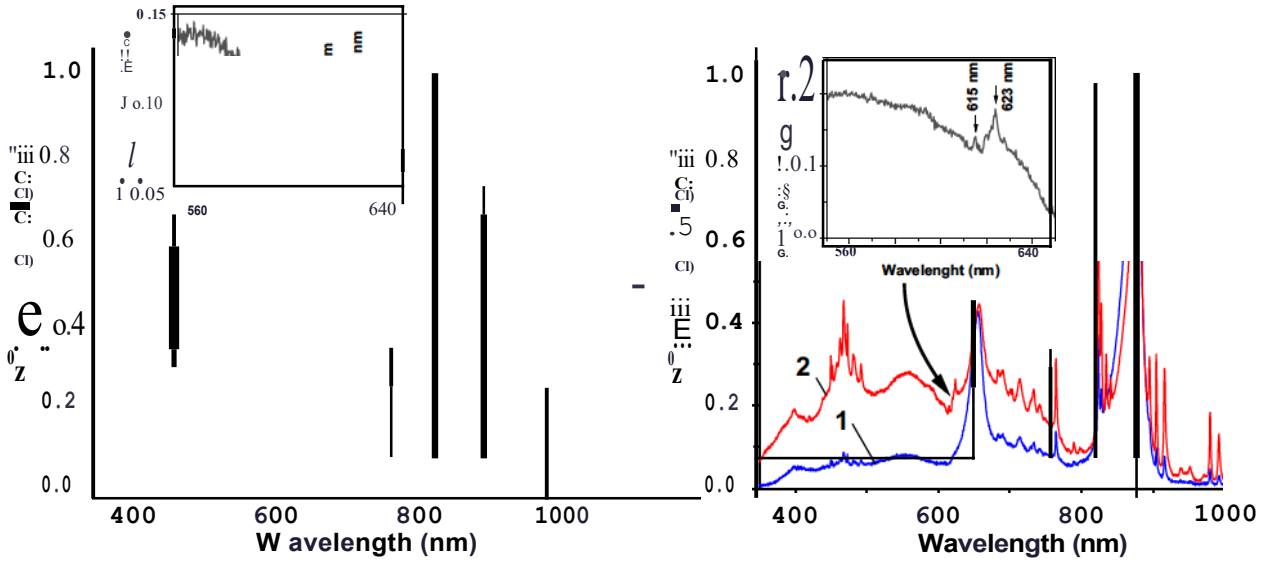

Figure11: Normalized (to the highest peak at 824nm) spectrum of the radiation of the solar simulator (AMO filter) reflected from (1) SHJ cell coated with two layers of CORIN and (2) SHJ cell coated with one layer of CORIN and SCL on the top. Zoom-in insert shows the difference between graphs 2 and 1 in the spectral region 550-650nm where the PL peaks at 615 and 623nm attributed to the SQ are visible.

Figure 12: Normalized (to the highest peak at 873 nm) spectrum of the radiation of the solar simulator {AMO filter) reflected from (1)!MM cell coated with CORIN and (2) IMM cell coated with SCL. Zoom-in insert shows the difference between graphs 2 and 1 in the spectral region 550-650nm where the PL peaks at 615and 623 nm attributed to the SCL are visible.

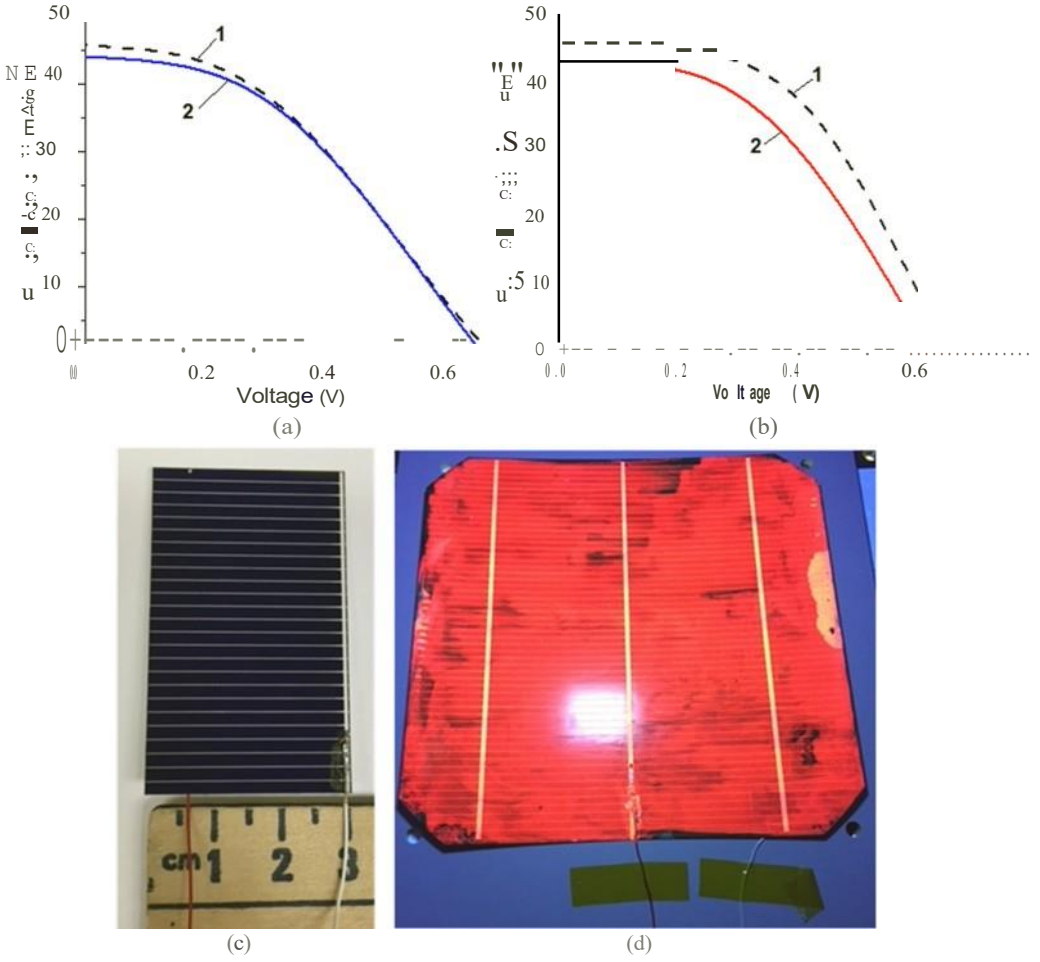

Figure 13: (a) *1-V* characteristics of an unexposed SHJ cell before coating (curve 1) and after coating with two layers of CORIN (curve2). (b) *1-V* characteristics of an unexposed SHJ cell before coating (curve1) and after coating with one layer of CORIN and SCL on the top (curve 2). During *I-V* measurements, the cells were illuminated by the solar simulator with an intensity equivalent to 1.367 Sun (AMO filter), the so-called solar constant - solar irradiance above the atmosphere. (c) General view of a bare SHJ cell. It was cut from an SHJ wafer. (d) An SHJ wafer coated with one layer of CORIN and SCL on the top illuminated with a 365nm UV LED. Red PL in (d) was produced by the SQ.

greater than the 15% spread. Correspon dingly, the same applied to *Pmax* and PDmax *(q* was proportional to Pmax and PDma-J As was verified by the reflectance measurements, both coatings reduced the so-called optical coupling of the incident light to the cells (6) or, in other words, increased the reflection of the incident light. This happened primarily because the polymer smoothened the surface texture of the cells intentionally etched to minimize reflectance. In the case of the SCL, another negative factor was the increased light scattering mentioned above (when the optical transmittance data in Figure 9 was discussed). The spectrum down-shifted PL didnot compensate for the loss of thevisible solar radiation reaching the cell.

We exposed theSHJ cellstolN radiationin vacuum (simulating solar lN in space) for a duration varying from 5,000 to 7,000 ESH, measured*I- V* characteristics for different exposure durations *t,* and extracted *Prrwo* PD= and *q* from each measured *I- V* characteristic. The change in *q* caused by lN exposure was evaluated using the dimensionless relative efficiency change Ar/re1= *(q* - q00 J x 100%'B b to compare different cells regardless of the absolute values of the efficiency; 'B b was the Beginning-of-Life (BOL) efficiency before exposure *(t* = 0 ESH). InTable1 qBoLis presented in thefourth column. Experimental plots of fil1re1 i5 duration *t* in ESH for the exposed cells are presented in Figure 14. Plots in Figure 14a and b were fitted with function fl'7re1(t> = [exp(Rt) - 1) x 100%, where fitting parameter *R* had the meaning of the efficiency evolution rate. Plot in Figure 14c was fitted with function fil1re1(t) = *A* (1- exp(Rit)I x 100%. The graphs of the fitting functions are presented by the sets of three lines: the middle, thicker lineis the evolution graphs corresponding to the mean values of the fitting parameters X !an (i = 1. 2, 3;X$ = *R, Jfl-1* = *A,* _x$ = *RJ.*

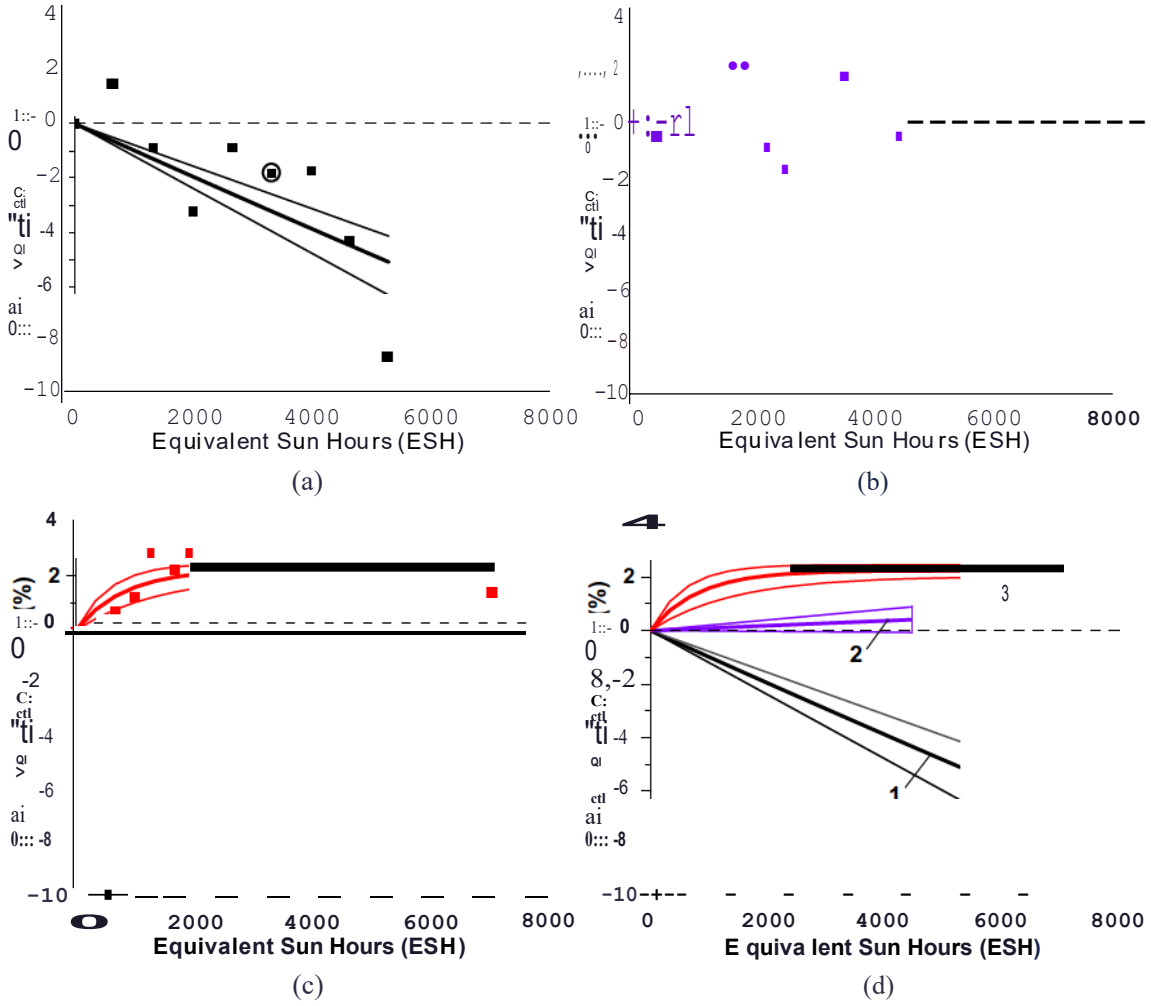

Figure 14: Experimental evolution plots of the relative efficiency change 6 f/£ ⅆ (a) bare SHJ cell, (b) SHJ cell coated with two layers of CORIN, and (c) SHJ cell coated with one layer of CORIN and SCL on the top. Solid lines are the graphs of the functions fitting the experimental points. The middle thick lines are the graphs of the fitting functions corresponding to the mean values of the fitting parameters. The marginal, thinner lines correspond to the marginal values equal to the mean values plus/minus standard deviations determined during fitting computations. Circles mark the experimental points corresponding to the data in Table 1 for ~3,000 ESH exposure duration. A square marks the experimental point corresponding to the data in Table **1** for ~6,000 ESH exposure duration. For convenience of comparison, fitting graphs for all the cells are presented together in (d). Set of fitting lines 1 corresponds to bare SHJ cell, Set of fitting lines 2 corresponds to SHJ coated with two layers of CORIN, and Set of fitting lines 3 corresponds to SHJ coated with CORIN and SCL on the top.

Two marginal thin lines on both sides from the middle are the graphs corresponding to the marginal values of the fitting parameters *xy>* and *x 0* equal to the mean values plus/minus the standard deviations *ax-0* of fitting *xf>* = X !an ± *ax-0*. For convenience of comparison, the fitting evolution graphs for all three types of the SHJ cells are presented together in Figure 14d. According to Figure 14, the uncoated SHJ cell experienced performance degradation (Figure 14a and evolution graph 1 in Figure 14d) while the CORIN-coated cell had a slight performance increase (Figure 14b and graph 2 in Figure 14d), and the SCL-coated cell got a performance increase followed by saturation (Figure 14c and graph 3 in Figure 14d). The evolution graphs (Figure 14d) are so different that their error margins do not overlap. The lN degradation of bare SHJ cells has been explained in the literature by an increase in hydrogen concentration near the Si/passivation interface and, as a result, a drop of short circuit current *Is,∴* and open circuit voltage *Voc* [SO]. Improved lN stability caused by CORIN (graph 2) could be a result of blocking lN by CORIN. The SCL-caused performance improvement (graph 3) could assumingly originate from the growing acceptance of lN solar light (confirmed by our measurements of the optical reflectance of the SCL-roated cells) and the downshifted PL (indicated by 615 and 623nm peaks in Figure 11).

Table 1: Performance parameters of the SHJ cells extracted from their *I-V* characteristics

Number of the row	Time of exposure	0 ESH		-3,000 ESH	-6,000 ESH
	Parameter	*Voe* (I,c) Uscl	Pmax (PDmaxl [q]"	Pmax (PDmaxl ['7]	P max (PDmaxl ['7]
	Unit	V (mA) [mA/cm^2]	mW (mW/cm^2) [%]	mW (mW/cm^2) [%]	mW (mW/cm^2) [%]
	Uncoated SHJ cell	0.681 ± 0.007 (708 ± 8) [45.3 ± 0.5]	176 ± 10 (11.3 ± 0.6) [10.5 ± 0.5]	173 ± 10b (11.1 ± 0.6) [10.2 ± 0.5]	17 0 ± 12< (10.9 ± 0.8) [10.0 ± 0.8]
2	SHJ cell before coating with two layers of CORIN	0.681 ± 0.007 (711 ± 8) (45.6 ± 0.5]	190 ± 10 (12.2 ± 0.6) (11.2 ± 0.5]	184 ± 11d (11.8 ± 0.6) (10.8 ± 0.6]	178 ± 13d (11.4 ± 0.8) (10.5 ± 0.8]
3	SHJ cell coated with two layers of CORIN	0.664 ± 0.007 (685 ± 7) (43.9 ± 0.4]	188 ± 10 (12.1 ± 0.6) (11.1 ± 0.5]	188 ± 10• (12.1 ± 0.6) (11.1 ± 0.5]	189 ± 11< (12.2 ± 0.7) (11.2 ± 0.7]
4	SHJ cell before coating with one layer of CORIN and one SCL on the top	0.654 ± 0.007 (645 ± 7) (46.2 ± 0.5]	211± 12 (15.1 ± 0.9) (13.9 ± 0.9]	204 ± 14d (14.6 ± 1.0) (13.4 ± 0.9]	1 99 ± 1r (14.3 ± 12) (13.1 ± 1.1]
5	SHJ cell coated with one layer of CORIN and one SCL on the top	0.681 ± 0.007 (604 ± 6) (43.3 ± 0.4)	180 ± 10 (12.9 ± 0.7) (11.8 ± 0.6)	189 ± 11[1] (13.5 ± 0.8) (12.3 ± 0.8)	184 ± 119 (13.2 ± 0.8) [12.1 ± 0.7]

•Efficiency was measured at an irradiance of 1.367 Sun (136.7mW/ cm^2) with AMO filter in the solar simulator and at the temperature in the labvarying between 22 and 27°C. It was corrected to the true efficiency that, according to ASTM E948-16 Standard (49], had to be measured at an irradiance of 1.0 Sun (100.0 mW/cm^2) with AM 1.5 G filter at a temperature of 25°C. bExact exposure time was 3,321 ESH. <Due to the lack of experimental data, the values were estimated using the results of fitting experimental data in Figure 14. dExpected values estimated using the results of fitting experimental data in Figure 14. •Exact exposure time was 3,147 ESH. [1]Exact exposure time was 2,981 ESH. 9Exact exposure time was 6,205 ESH.

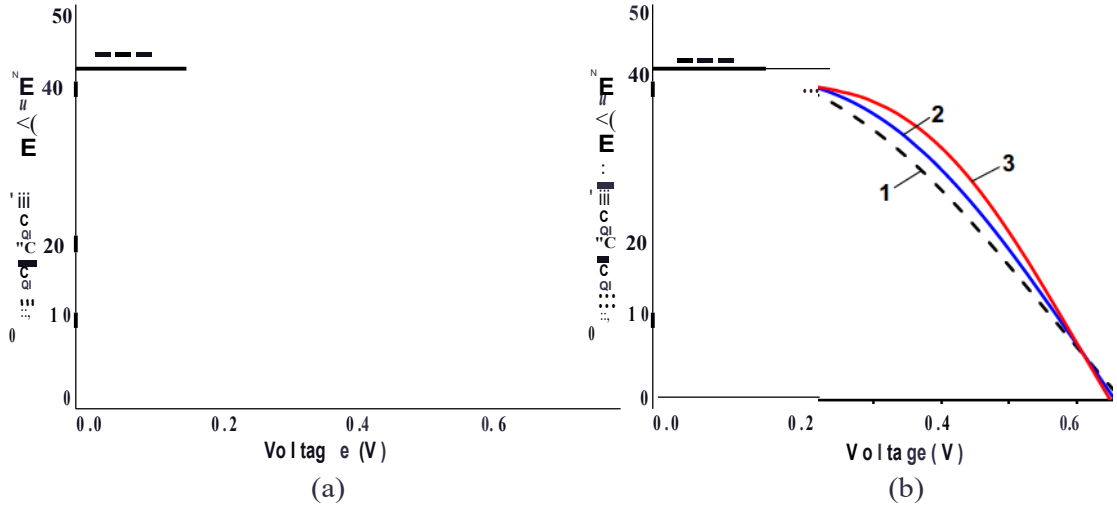

Figure 15: *I-V* characteristics of three different SHJ cells (a) before UV exposure and (b) after UV exposure for -3,000 ESH. Curve 1 corresponds to the bare cell, curve 2 corresponds to the cell coated with two layers of CORIN, and corresponds to curve 3 corresponds to the cell coated with one layer of CORIN and SCL on the top. Actual exposure time of the bare cell was 3,321 ESH, CORIN-only-coated cell - 3,147 ESH, CORIN+ SCL-coated- 2,981 ESH. During *I-V* measuremetns, the cells were illuminated by the solar simulator with an intensity of 1.367 Sun (AMO filter) .

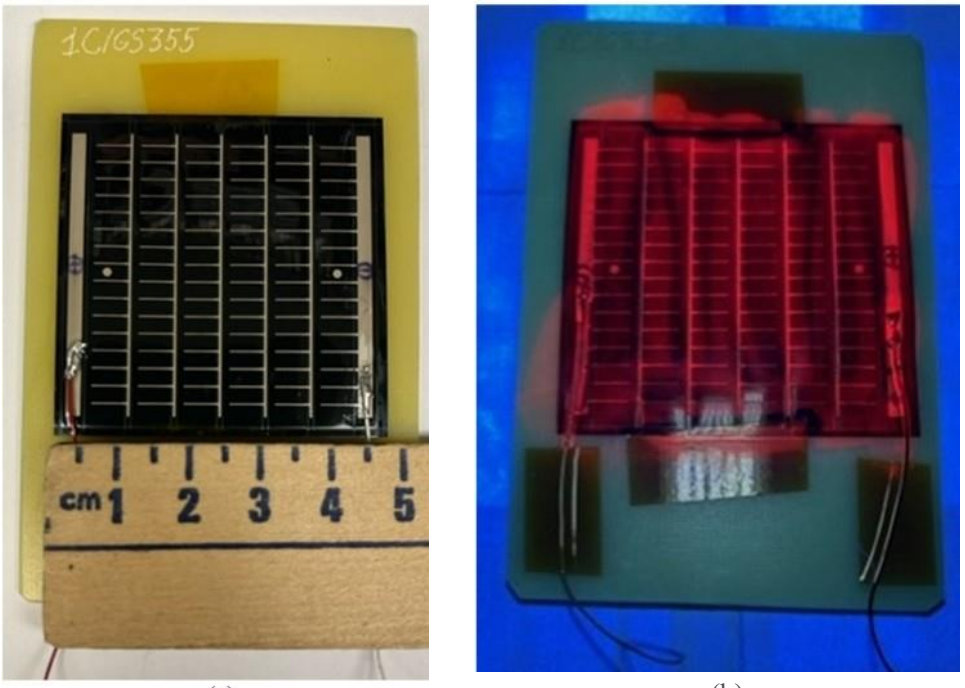

Figure16: (a) General view of a CIGS cell coated with SCL. (b) The same cell illuminated with UV light from a 365 nm UV LED. Red PL was produced by the SQ.

We also compared the *I- V* characteristics of three different SHJ cells, bare, double CORIN-, and CORIN + SCL-coated, before and after UV exposure for ~3,000 ESH as shown in Figure 15. The values of *Pmax,* PDmax, and *'I* extracted from these characteristics are presented in Table 1, columns 4 and 5, rows1, 3, and 5.The corresponding experimental points of AIJre1 we re marked with circles in the plots in Figure 14a- c. They were located (with the exception in Figure14a) close to the fitting graphs. The bare cell initially performed less than the other two, and the CORIN + SCL-

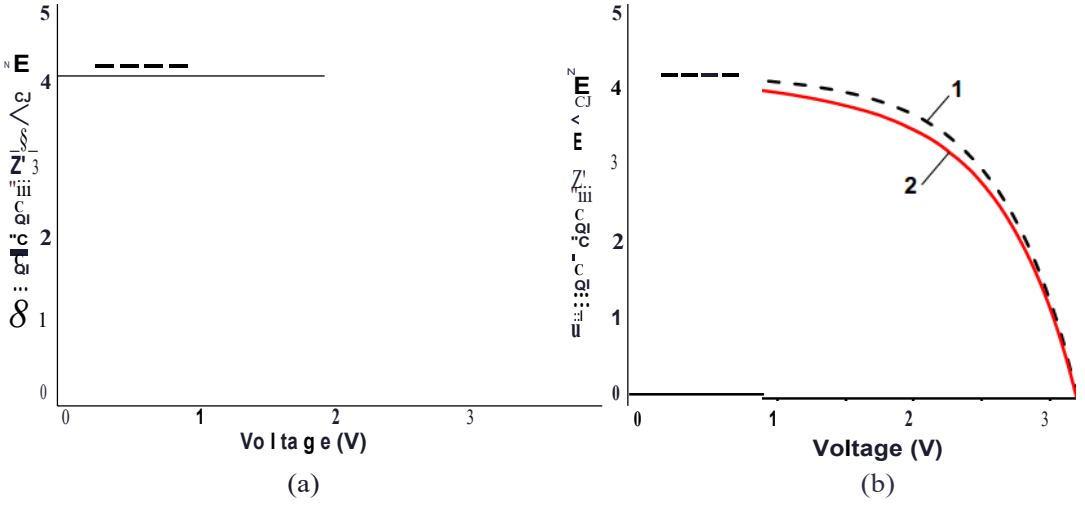

Figure17: (a) *1-V* characteristics of an unexposed CIGS cell before coating (curve 1) and after coating with CORN layer (curve 2). (b) *1-V* characteristics of an unexposed CIGS cell before coating (curve 1) and after coating with SQ (curve2). During *1-V* measuremetns, the cells were illuminated by the solar simulator with an intensity of 1.367 Sun (AMO filter). After the article was prepared for publication the manufacturer of CIGS cells suggested that the active area of the cell was 17.77 cm^2 instead of 22.5625 cm^2 used in the computations. Correspondingly, the current density in (a) and (b) should be increased 1.27 times.

coated one was the highest achiever. After - 3,000 ESH of exposur e, the performance gap between the underperformer (bare cell) and the frontrunner (CORIN +SCL-coated one)widened. The performance of the CORIN-coated cell did not noticeably change. Using the available experimental data or the estimates derived from the fitting functions in Figure 14 (if the experimental data were not available,) we also obtained the performance parameters of three SHJ cells for -6,000 ESH exposure duration. They are presented in Table1, sixth column, rows1, 2, and 4. The corresponding experimental point of 'lrel wasmarked with a squarein the plotin Figure14c. Itwas located closeto the fitting graph The gap between the performance parametersofthe bare cell and the CORIN-only and CORIN-SCL cells continued to widen. However, the change in the performance of individual cells with time was less or comparable to the statistical spread (statistically insignificant). Comparison of the expected performance parameters of the would-b coated cells (that were double CORIN- or CORIN+ SCL-coated) for -3,000 and -6,000 ESH in Table1, columns 5 and 6, rows2 and **4** with the parameters of the true uncoated cell in row 1 show their correlation in terms of degradation with exposure time.

Figure 16 presents the photographs of an SCL-coated CTGS cellilluminated with room and lN light.SCL beinglN illuminated produced red PL attributed to the Europium doped downshifting NPs. The *I- V* characteristics of the CIGS cells , uncoated and coated, befor e lN exposure are presented in Figure17. The performance parameters of the cells are presented in Table 2, columns 3 and **4,** rows 2 through 5. In this case, CORIN coating brought a slight increase in *'I* (by 0.4%) with respect to the bare cell. SCL reduced *'I* by 0.4%. But these changes in perform ance in

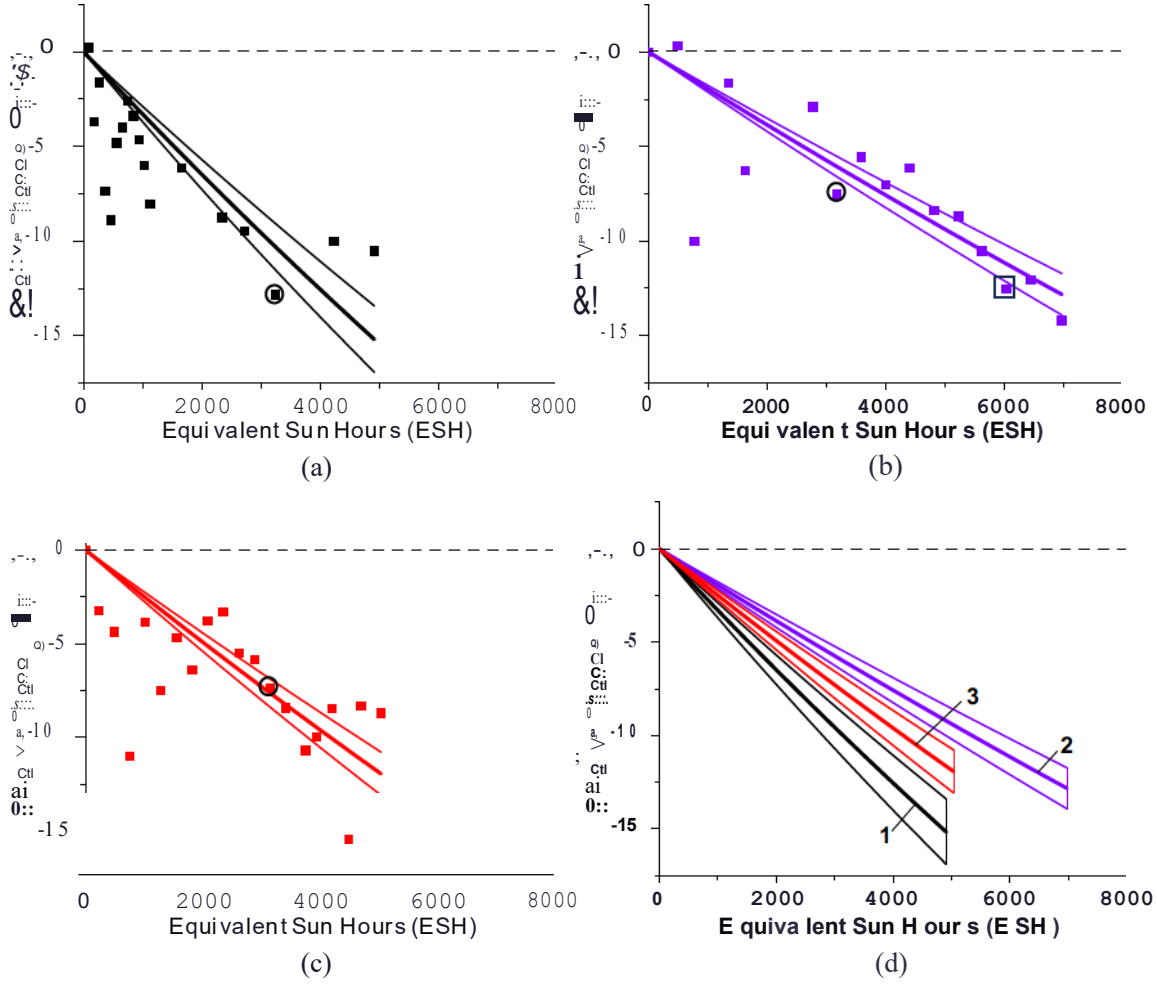

Figure 18: Experimental evolution plots of the relative efficiency change flr/,e1 of (a) bare CIGS cell, (b) CIGS cell coated with CORIN, and (c) CIGS cell coated with SCL. Solid lines are the graphs of the functions fitting the experimental points. Orcles mark the experimentaploints corresponding to the data in Table 2 for ~3,000 ESH exposure duration. A square marks the experimental point corresponding to the data in Table 2 for ~6,000 ESH exposure duration. (d) For convenience of compariso,nfitting graphs for all the cells are represented together in. Setoflines 1 corresponds to bare CIGS cell, while 2 corresponds to CIGS coated with CORN, and 3 corresponds to OGS coated with SQ.

both cases are less than 1.0% statistical spread of *q*. The effect of the coatings on the performance of unexposed CIGS cells could thus be considered statistically insignificant.

After the article was prepared for publication the manufacturer of CIGS cells suggested that the active area of the cell was 17.77 cm^2 instead of 22.5625 cm^2 used in the computations. Correspondingly, the current density in Figure 17 and Table 2 as well as power density and efficiency in Table 2 should be increased *127* times.

Experimental evolution plots of ru,,ei of the UV-exposed CIGS cells are presented in Figure 18. All the plots were fitted with function *IIfJ,e1Ct)* = [exp(Rt) - 1) x 100%, where fitting parameter *R* had the meaning of the efficiency evolution rate. Like in Figure 14, the graphs of the fitting functions were presented by the sets of three lines: the middle, thicker line and two thin marginal lines corresponding to the marginal values of *R*± equal to the mean value Rmean plus/minus the standard deviations *aR* of fitting *R*± = Rmean ± *a R*. For convenience of comparison, the fitting evolution graphs for all three types of CIGS cells were presented together in Figure 18d. The uncoated CIGS cell (Figure 18a and set 1 in Figure 18d) experienced significant performance degradation while the CORIN-coated (Figure 18b and set 2 in Figure 18d) and SCL-coated (Figure 18c and set 3 in Figure 18d) cells degraded less. UV caused performance degradation of the bare CIGS cell (Figure 18a and set 1 in Figure 18d) was explained in the literature by the erosion of the front electric conductors followed by the increase in their sheet resistance (51.) Photographs of the microscopic images of the front conductors of the studied CIGS cells in Figure 19e-h confirmed this hypothesis. UV exposure of the bare front conductors of SHJ (Figure 19a-d) and IMM cells (Figure 19i-l) resulted in fluffy edges. But the white electroconductive (made of silver paste) layer of the front conductor of a bare CIGS cell (Figure 19e) completely changed its color to dark yellow after ~5,000 ESH of UV exposure (Figure 19f). This was more likely due to oxidation of silver. The CORIN-coated CIGS cell remained almost intact after ~ 7,000 ESH (Figure 19g). The conductor of the SCL-coated cell remained partially intact after ~ 5,000 ESH (Figure 19h). Slowing UV degradation down by CORIN and the SCL could thus be due to counter-UV shielding of the front conductors. The fact that the SCL provided weaker shielding of the front conductors than CORIN explains why the SCL-coated cell degraded a bit faster (but still slower than the bare cell). The SCL was less effective on the CIGS technology more likely due to the formation of pinholes in the

Table 2: Performance parameters of the CIGS cells extracted from their *1-V* characteristics•

Number of the row	Time of exposure	0 ESH		-3,000 ESH	-6,000 ESH
	Parameter	*Voe* (l,cl *U,d*	Pmax (PDmaxl [IJ)	Pmax (PDmaxl [IJ)	Pmax (P D maxl [IJ)
	Unit	V (mA) [mA/ cm^2J	mW (mW/ cm^2) [%)	mW (mW/cm^2) [%]	mW (mW/cm^2) [%]
	Uncoated CIGS cell	3.14 ± 0.09 (92.4 ± 1.9) [4.10 ± 0.09)	155 ± 11 (6.8 ± 0.5) (6.2 ± 0.4)	135 ± 10' (5.9 ± 0.4) (5.4 ± 0.3)	137 ± 13b (6.0 ± 0.6) (5.5 ± 0.5)
2	CIGS cell before coating with CORIN layer	3.34 ± 0.10 (98.8 ± 2.0) [4.38 ± 0.09)	179 ± 13 (7.9 ± 0.6) (7.2 ± 0.5)	162 ± 15< (7.1 ± 0.7) (6.5 ± 0.6]	146 ± 17' (6.4 ± 0.7) [5.9 ± 0.7]
3	CIGS cell coated with CORIN layer	3.41 ± 0.10 (97.4 ± 2.0) [4.32 ± 0.09]	185 ± 14 (8.2 ± 0.6) (7.6 ± 0.5]	171 ± 13d (7.6 ± 0.6) (7.0 ± 0.5]	162 ± 12• (7.2 ± 0.5) [6.7 ± 0.5]
4	CIGS cell before coating with SCL	3.20 ± 0.09 (95.6 ± 2.0) [4.24 ± 0.09]	173 ± 13 (7.7 ± 0.6) (7.1 ± 0.5]	156 ± 15< (6.9 ± 0.7) [6.4 ± 0.6]	142 ± 17< (6.3 ± 0.8) [5.8 ± 0.7]
5	CIGS cell coated with SCL	3.19 ± 0.09 (93.4 ± 1.9) [4.14 ± 0.08]	163 ± 12 (7.2 ± 0.5) [6.7 ± 0.5]	151 ± 11t (6.7 ± 0.5) [6.2 ± 0.5]	143 ± 14b (6.3 ± 0.6) [5.9 ± 0.6]

•oue to the corrections provided by the manufacturer after the article was prepared for publication current density *}s,c,* power density *PDmax,* and efficiency *IJ* must be increased 1.27 times. •Exact exposure time was 3,245 ESH. bDue to the lack of experimental data, the values were estimated using the results of fitting experimental data in Figure 18. <Expected values were estimated using the results of fitting experimental data in Figure 18. dExact exposure time was 3,176 ESH. •Exact exposure time was 6,037 ESH. fExact exposure time was 3,126 ESH.

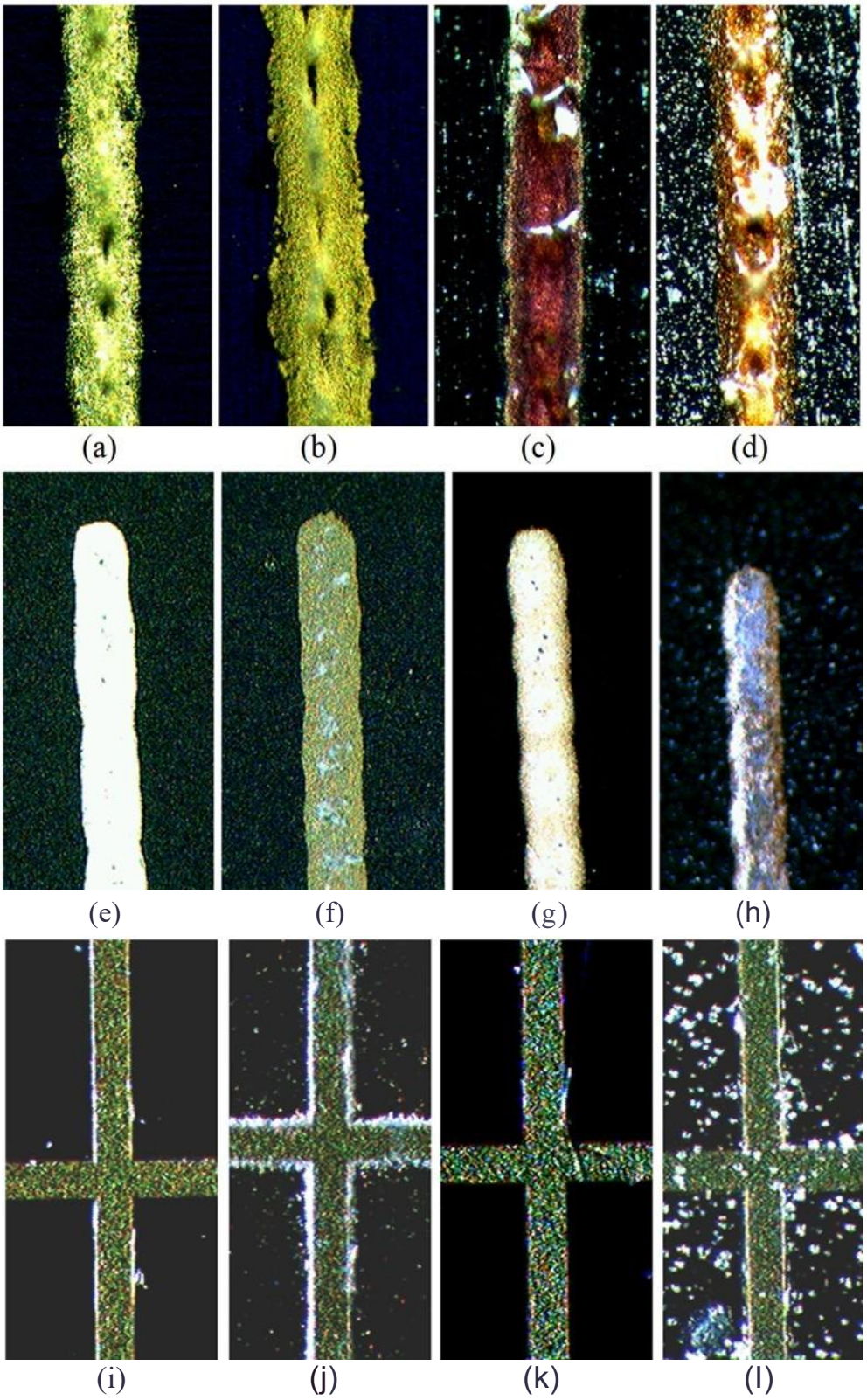

Figure 19: Microscopic images (40x magnification) of the front conductor of (a) bare unexposed SHJ cell, (b) bare SHJ cell UV-exposed for 5,294 ESH, (c) SHJ cell coated with two layers of CORIN and UV-exposed for 4,453 ESH, (d) SHJ cell coated with one layer of CORIN and SCL on the top and UV-exposed for 7,058 ESH, (e) bare unexposed CIGS cel,l (f) bare CIGS cell UV-exposed for 4,913 ESH, (g) CORIN-coated CIGS cell exposed for 6,977 ESH, (h) SCL-coated OGS cell exposed for 5,038 ESH, (i) bare unexposed **IMM** cell, 0) bare **IMM** cell UV-exposed for 6,870 ESH, (k) CORIN-coated IMM cell exposed for 6,736 ESH, and (I) SCL-coated **IMM** cell exposed for 5,693 ESH. Images (e)-(h) are enlarged -1.5 times with respect to images (a)-(d), images (i)-{l) are enlarged -2 times.

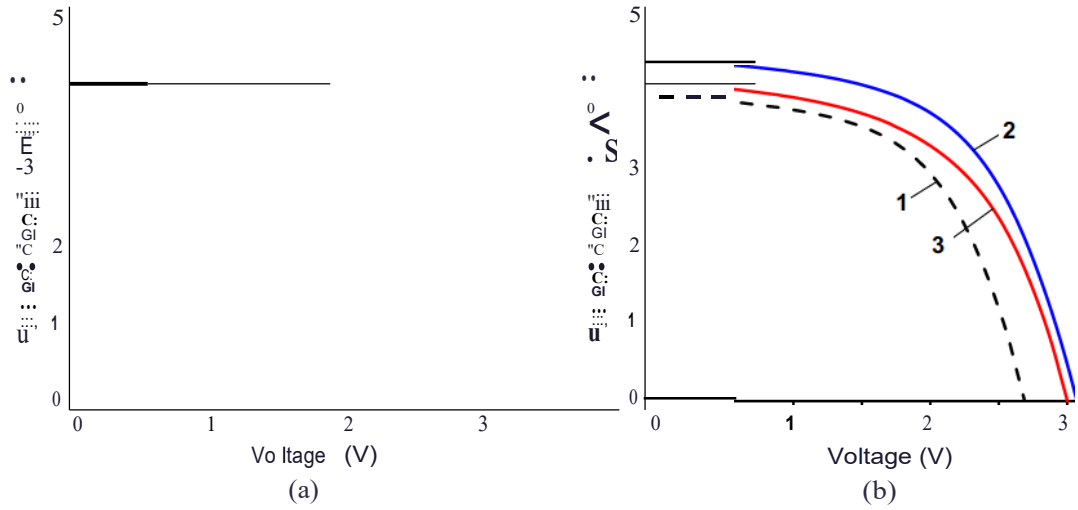

Figure 20: *I-V* characteristics of three different CIGS cells (a) before UV exposure and (b) after UV exposure for ~3,000 ESH. Curves 1 correspond to the bare cell, curves 2 correspond to the cell coated with one layer of CORIN, and curves 3 correspond to the cell coated with the SCL. The actual exposure time of the bare cell was 3,245 ESH, CORIN-coated cell was 3,176 ESH, and SCL-coated cell was 3,126 ESH During *I-V* measurements, the cells were illuminated by the solar simulator with an intensity of 1.367 Sun. Due to the corrections provided by the manufacturer after the article was prepared for publication, current density in (a) and (b) must be increased 1.27 times.

CORIN because of the NP deposition, which would re-expose the silver top contacts. The silver contacts on the CIGS only experienced degradation due to the lack of a protective coating, as evidenced by the CORIN coated module. SHJ and IMM cells might have initial anti-IN coating preventing front conductors from complete degradation.

We also compared the *I-V* characteristics of three different CIGS cells, bare, CORIN-, and SCL-coated, before and after IN exposure for ~3,000 ESH as shown in Figure 20. Due to corrections provided by the manufacturer, the current density in Figure 20 should be increased 1.27 times. The values of *Pmax*, PD= and *q* extracted from these characteristics are presented in Table 2, columns 4 and 5, rows 1, 3, and 5 (they must also be increased 1.27 times). Relative change illlret was negative for all three types of cells due to IN-induced aging, but the performance gap between the exposed bare CIGS cell and the coated cells (especially the CORIN-coated one) widened. Additionally we put the experimental data for the

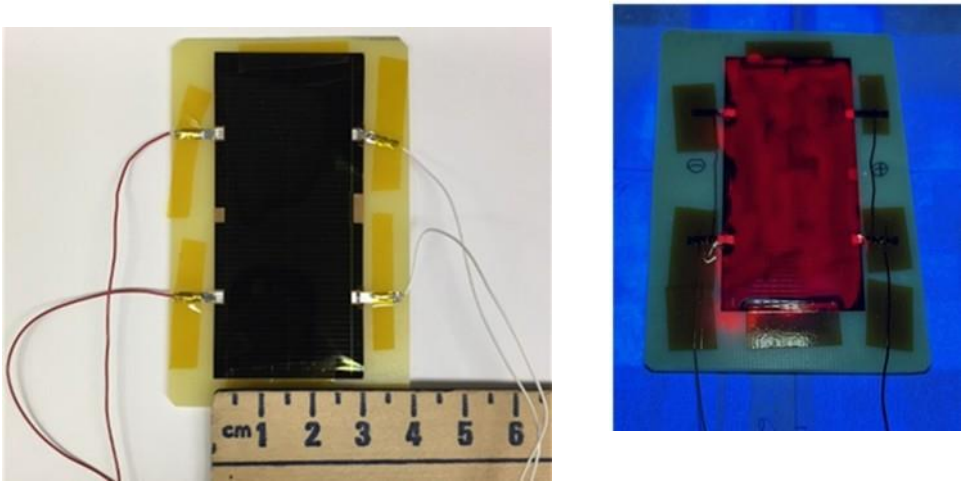

(a) (b)

Figure 21: (a) General view of a bare IMM cell from Microlink; (b) an SCL-coated IMM cell illuminated with a 365nm UV LED. Red PL in (b) was produced by the SQ.

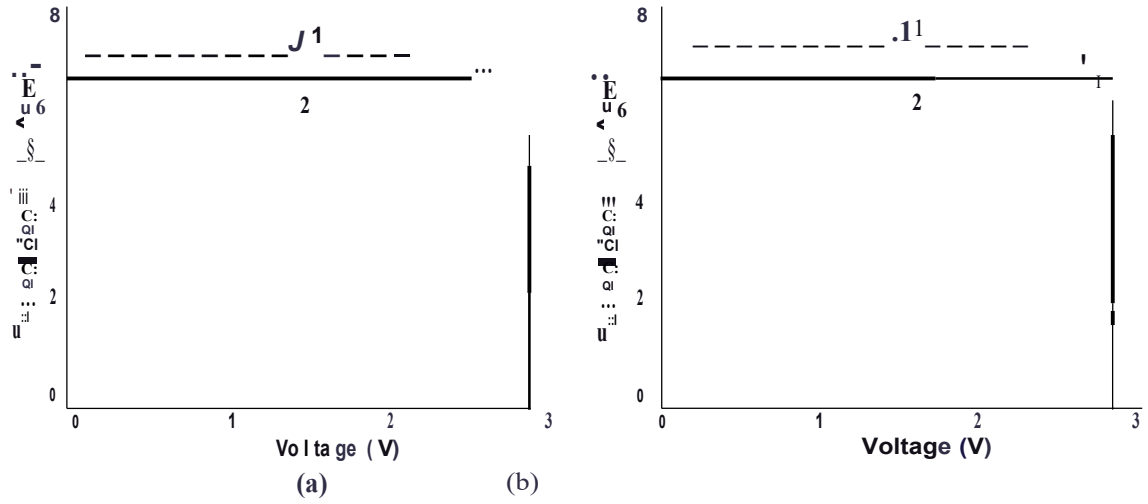

Figure 22: (a) *1-V* characteristics of an unexposed **I MM** cell before coating (curve 1) and after coating **with** one layer of CORIN (curve 2). (b) *1-V* characteristics of an unexposed **IMM** cell before coating (curve 1) and after coating with the SCL (curve 2). Considering greater (relative to SHJ and CIGS) IMM cell dimensions (3.0 cm x 6.6 cm), the cells were illuminated at a maximal achievable for the solar simulator irradiance of 0.875 Sun (AMO filter). This was less than 1.367 Sun used for SHJ and CIGS cells.

Table 3: Performance parameters of the **IMM** cells extracted from their *1-V* characteristics

Number of t he row	Tim e **of exposure**	0 ESH		-3,000 ESH	-6,000 ESH
	Parameter	*Voe* (I, J *U•.J*	P mu (PDmaxl 111·	Pmu (PDmaxl I'll	P max (P Dmul I'll
	Unit	V (mA) [mA/cm²J	mW (mW/cm²) [%]	mW (mW/cm²) [%]	mW (mW/cm²) [%]
	Uncoated **IMM** cell	2.91 ± 0.02 (143.5 ± 2.4) [7.23 ± 0.12]	376 ± 13 (18.9 ± 0.7) [27.2 ± 1.0]	365 ± 13b (18.4 ± 0.7) (26.5 ± 1.0]	364 ± 13< (18.3 ± 0.7) (26.4 ± 0.9]
2	**IMM** cell before coating with CORIN layer	2.88 ± 0.02 (140.1 ± 2.3) [7.07 ± 0.12]	353 ± 13 (17.8 ± 0.7) (25.6 ± 1.0]	346 ± 14d (17.4 ± 0.7) (25.1 ± 1.0]	336 ± 16d (17.0 ± 0.8) (24.4 ± 1.1]
3	**IMM** cell coated with CORIN layer	2.93 ± 0.02 (132.3 ± 2.1) (6.68 ± 0.11]	339 ± 12 (17.1 ± 0.6) (24.6 ± 0.9]	327 ± 12" (16.5 ± 0.6) (23.8 ± 0.9]	321 ± 1it (16.2 ± 0.5) (23.3 ± 0.9]
4	**IMM** cell before coating with SCL	2.89 ± 0.02 (144.9 ± 2.3) [7.32 ± 0.12]	*3n* ± 13 (19.0 ± 0.7) [27.3 ± 1.0]	369 ± 15d (18.6 ± 0.8) (26.7 ± 1.1]	359 ± 16d (18.1 ± 0.8) (26.1 ± 1.1]
5	**IMM** cell coated with SCL	2.91 ± 0.02 (134.1 ± 2.2) [6.n ± 0.111	350 ± 13 (17.7 ± 0.7) [25.5 ± 1.0]	350 ± 129 (17.7 ± 0.6) (25.5 ± 0.9]	351 ± 16h (17.8 ± 0.8) [25.6 ± 1.2]

•Efficiency was measured at an irradiance of 0.875 sun (87.5 mW/cm 2) with AMO filter in thesolar simulator and at the temperature in the lab varying between 22 and 27°C. It was corrected to the true efficiency based on ASTM E948-16 Standard (49]. bExact exposure time was 3,026 ESH. <Exact exposure time was 6,269 ESH. dExpected values were estimated using the results of fitting experimental data in Figure 23. •Exact exposure time was 3,020 ESH. [Exact exposuretime was 6,037 ESH. 9Exactexposure time was 3,298 ESH. hDueto the lack of experimental data,the values wereestimated using the results of fitting experimental data in Figure 23.

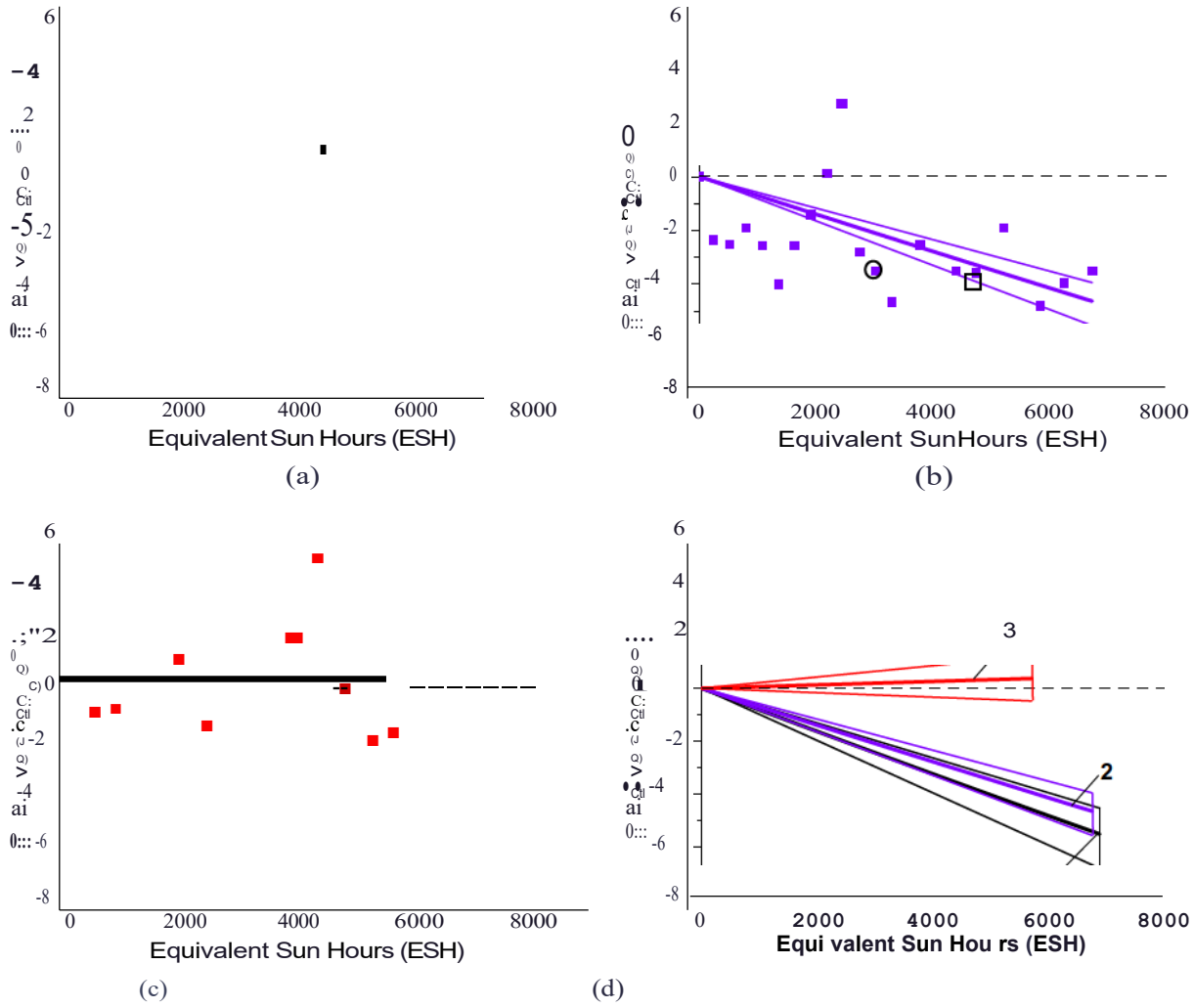

Figure 23: Experimental evolution plots of the relative efficiency change η/η_0 of (a) bare IMM cell, (b) IMM cell coated with CORIN, and (c) **IMM** cell coated with SCL. Solid lines are the graphs of the functions fitting the experimental points. Circles mark the experimental points corresponding to the data in Table 3 for -3,000 ESH exposure duration. Squares mark the experimental points corresponding to the data in Table 3 for - 6,000 ESH exposure duration. (d) For convenience of comparison, fitting graphs for all the cells are presented together. Set of lines 1 corresponds to bare IMM cell, while 2 corresponds to **IMM** coated with CORIN, and 3 corresponds to **IMM** coated with SCL.

CORIN-coated CTGS cell exposed for - 6,000 ESH (data point marked with a square in Figure 18b) and the performance parameters of the would-be-uncoated and the true uncoated and coated cells for - 3,000 and - 6,000 ESH (estimated using the fitting functions in Figure18) in Table 2, columns 5 and 6, rows 1- 5. The data for the would-be-uncoated and the true W1coated cells showed good correlation.

Figure 21shows the photographs of a bare IMM cell at room illumination and the SCL-coated one under lN illumination. SCL on the top of the latter cell produced red PL attributed to the spectrum downshifting in the embedded NPs. The *I- V* characteristics of the IMM cells, uncoated and coated, before UV exposure are presented in Figure 22. The performance parameters of the cells extracted from the *I- V* characteristics are presented in Table 3, columns 3 and 4, rows 2- 5. Both coatings brought down the photocurrent and the efficiency of the cells (though not significant relative to the statistical spread). Like in the case of the SHJ cells, reflectance measurements indicated that the coating-caused performance drop could be due to the increased reflection and scattering (especially in the case of the SCL) of the incident light.

Figure 23 presents the experimental evolution plots of η/η_0 of the UV-exposed IMM cells. All the plots were fitted with function $\eta/\eta_0(t) = [\exp(Rt) - 1] \times 100$ (%), with evolution rate *R* as a fitting parameter. Like in Figures 14 and 18, the graphs of the fitting functions were presented by the sets of three lines: the middle, thicker line and two thin

marginal lines corresponding to the marginal values of *R*. For convenience, the fitting evolution graphs for all three types of IMM cells are presented together in Figure 23d. The uncoated IMM cell (Figure 23a and set 1 in Figure 23d) experienced performance degradation. The CORIN-coated (Figure 23b and set 2 in Figure 23d) experienced slightly less degradation while the SCL-coated one (Figure 23c and set 3 in Figure 23d) demonstrated performance stability.

Figure 24 presents the *I- V* characteristics of different bare, CORIN-, and SCL-coated **IMM** cells before and after lN exposure for -3,000 ESH. The short circuit current density]se of the bare cell remained relatively high and stable before and after exposure. But the open circuit voltage $V_{0}e$ of the bare cell as well as that of the CORIN-coated one degraded compared to the SCL-coated cell. Our measurements revealed that the SCL-coated cell reflected solar lN three to five times greater than the CORIN-coated and bare one, respectively. The stabilizing effect of the SCL on the IMM cell could thus be explained by fending off solar lN and keeping $V_{0}e$ from decreasing. Downshifted PL (indicated by 615 and 623nm peaks in the spectrum in Figure 12) could also contribute to the SCL's performance stabilizing role in the case of an IMM cell. The drop of V_{oe} in PV cellshas been explained in the literature bythe generation of parasitic defect-related traps in the energy gap of the p- n junctions (our IMM cells had three p- n junctions) and narrowing the gap (52]. Answering why such phenomena took place in our case would require detailed investigation beyond the scope of this work. The values of P_{max}, PDmax,

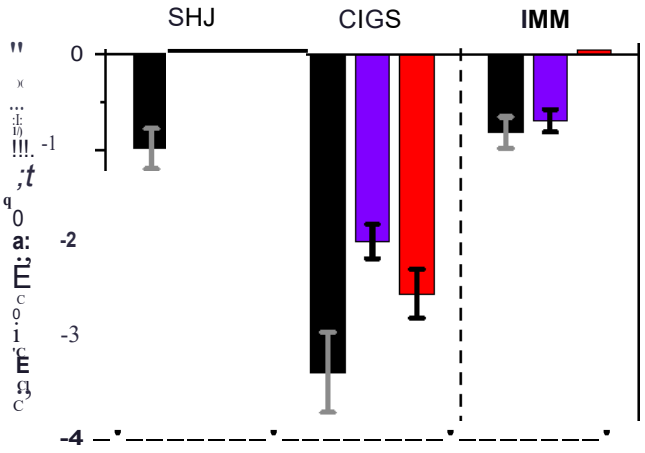

Figure 25: Chart diagram of the rates of the relative efficiency change IY],.1 of the uncoated and coated solar cells studied in this work. The bars of black color (left from the center of each solar cell group) correspond to the bare cells, blue bars (center) correspond to CORIN-coated (two layers of CORIN in the case of SHJ) cells, red (right from the center) correspond to SCL-coated (CORIN layer and SQ on the top in the case of SHJ) ones. The error bars are represented by thin grey/black lines. Thin bars near zero correspond to the cases when there is no efficiency degradation of the cells.

and *11* extracted from *1- V* characteristics in Figure 24 are presented in Table 3, columns 4 and 5, rows 3 and 5. Additionally, we put the experimental data for the bare and CORIN-coated IMM cells exposed for -6,000 ESH (data points marked with squares in Figure 23a and b) and the performance parameters of the would-be-uncoated and the true uncoated and coated cells for -3,000 and - 6,000 ESH

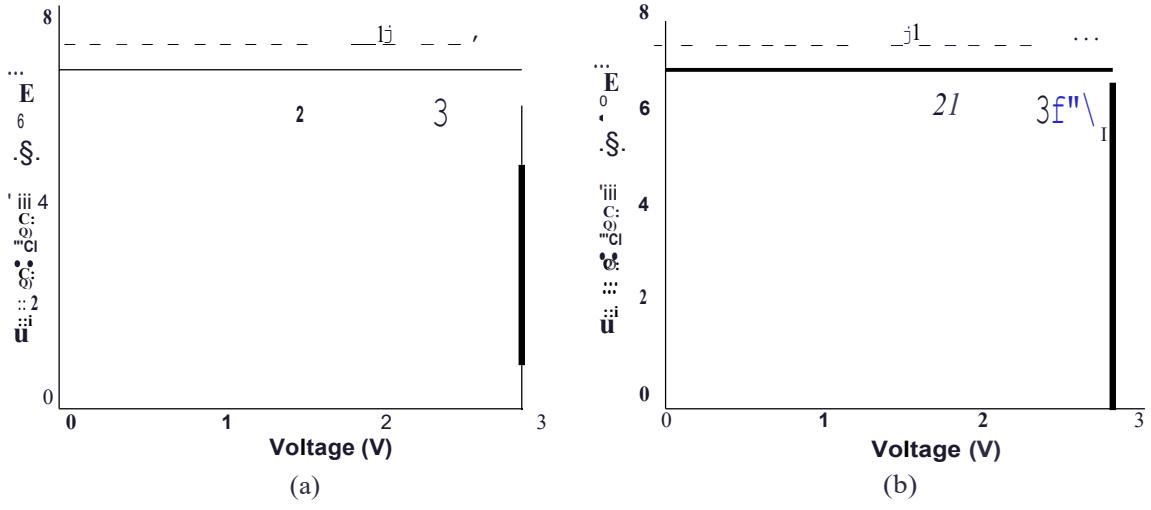

Figure 24: 1-Vcharacteristicsof three different IMM cells (a) beforeUV exposure and(b) after UV exposure for -3,000ESH. Curves 1 correspond to the barecell,curves 2 correspond to the cellcoated with onelayer of CORIN, and rurves3 correspond to the cell coated with the SCL. The actual exposure time of the bare cell was 3,026 ESH, while the CORIN-coated cell was3,020 ESH and SCL<oated was 3,298 ESH. During *I-V* measurements, the cells were illuminated by the solar simulator with an intensity of 0.875 Sun.

Table 4: Degradation rates of the t.l],.,, of the UV exposed solar cells

Type of solar cell	UV degradation rate R of 41J,e1 (ES-H^{1}) x 10-6		
	No coating	CORIN	SCL
SHj'	-(9.9 ± 2.1)	No degradation	No degradation
GGS	-(33.5 ± 4.2)	-(19.7 ± 1.8)	-(25.2 ± 2.6)
IMM	-(8.2 ± 1.7)	-(7.0 ± 1.2)	No degradation

•rn the case of SHJ cells, "CORIN" coating meant two layers of CORIN and "SCL" coating meant one layer of CORIN and SCL on the top.

(estimated using the fitting functions in Figure 23) in Table 3, columns 5 and 6, rows 1- 5. The data for the would-be-uncoated and the true uncoated cells correlated well in terms of performance degradation with time of exposure.

In summary, Figure 25 presents the chart diagram of the degradation (negative) rates of the relative efficiency change *llrJrel* of all the investigated solar cells. Thin bars near zero correspond to the cases when there was no efficiency degradation of the cells. The rates are also presented in Table 4. All the bare cells tended to degrade

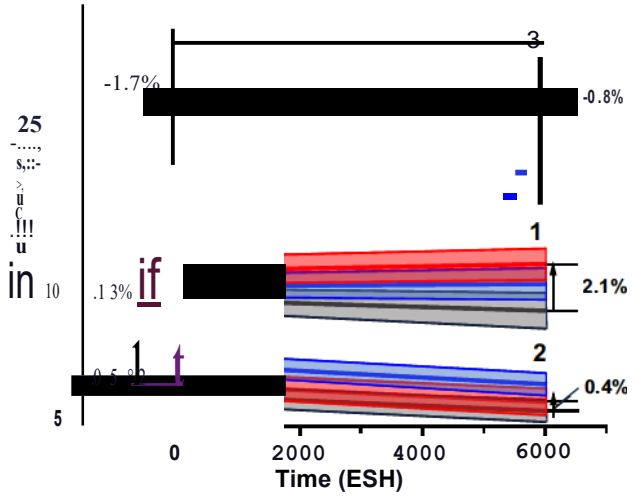

Figure 26: Evolution of the efficiency 'I of (1) SHJ, (2) GIGS, and (3) IMM cells with the time of UV exposure. Grey bars correspond to the uncoated cells, while blue bars correspond to the cells coated with CORIN (two layers of CORIN in the case of SHJ cell) and red bars correspond to the cells coated with SCL (CORIN layer and SCL on the top in the case of SHJ cell). The middle thick lines inside the bars correspond to the average efficiency. The border lines of the bars mar1< the statistical spreads. The graph is constructed by aggregating the data of Tables 1-3. Numerical values on both sides of the bars are equal to difference 6f/ between the efficiency of the SCL-coated cells 'l(sa.i and the efficiency of the bare cells „hiar•l : 6f/ = 'l(Sc - „hiar_•l Vertical arrows up correspond to positive 6f/, arrows down correspond to negative 6f/. Due to the corrections provided by the manufacturer after the artide was prepared for publi cation, the current density efficiency 'I of CIGS cells must be increased 27 times.

under UV exposur e. Bare IMM had the lowest degradation rate. CIGS cells , even coated, were prone to the fastest degradation probably due to UV-activated erosion of the front conductors. However , there might be a complication to account for that depends on the layer structure and composition of a particular type of CIGS. This relates to the UV/deep-blueactivation or "boosting" of the front ZnO layer (s) which need UV to be sufficiently conductive (53).CORIN or SCL might slow down the erosion of the front conductor by blocking UV but increase the loss of the UV-acti vated fr ont ZnO conductivity . In the case of the CIGS cells used in this study, the front layer was indium tin oxide.

The performance stabilizing effect of the SCL was observed for all thr ee types of cells and always beyond the statistical spread of the rate. For the SHJ and IMM cells, the SCL turned degradation into zero or slight growth. For the CIGS cell, the SCL reduced the degradation rate by - 25%. For the CIGS cell, CORIN performed as a better stabilizer than the SCL.

The data in Tables1- 3, columns 4 and 6 are aggregated and presented in Figure 26in the form of schematic evolution plotsof the efficiency 'I of all three types of solar cells. Numb ers to the left from the plots are equal to the differences Of/B ϕ between the Beginning-of-Life (BOL) efficiencies „$_{BOL}$ L) and 'l$_{BOL}$ (bare) of the SCL-coated and bare cells, respectively: Of/BOL = 'l ri L) · 1 ri re>. Numb ers to the ri ght are equal to the difference between the End-of-Life (EOL) efficiencies (after 6,000 ESH or -1.37 years of UV exposure): Of/E ϕ = „g L) · 1 e) The best improvement over time due to SCL in term s of absolute value of efficiency was in the case of IMM cell: Of/B/ dL was - 1.7% (negative due to initial deposition of SCL according to Figure 22b and the data in Table 3, column **4,** rows **4** and 5) and grew up by 0.9% to Of/EoL = - 0.8%. It could be expected that after -12,000 ESH, the efficiency will break even (8fE/ dL will become zero), *i.e,.* the initial efficiency loss due to SCL will be compensated by the efficiency gain over time. In the case of SHJ cell, Of/BoL was1.3%and grewup by 0.8%to OfE/ dL = 2.1 %. According to Figure 13b and the data in Table 1, column **4,** rows **4** and 5, Of/BoL would be expected to be negative due to SCL. But, as can be seen from the data in Table 1, column **4,** rows 1, 4, and 5, because of the natural random variation, the efficiency of a particular uncoated SHJ cellturned out to be sohigh (row **4** compared to row1) that Of/B/ dL r e main ed positive even after SCL deposition. In the case of GIGS OfE/dL (based on the experimental data) dropped by 0.1% with respect to Of/B/OL· In the case of **IMM,** the efficiency growth was slightly greater than the statistical spread (the width of the evolution bars). For the other two types, it was less or comparable to the spread.

It must be mentioned that the SCL can also potentially protect solar cells from high-energy particles (electrons and protons) in space. The study of these features will be conducted soon.

4 Conclusion

The obtained results indicated that a polymer nanocomposite SCL made of a colorless and atomic-oxygen-stabilized polyimide with the embedded NPs of an Eu-doped fluoride could improve the UV stability of the coated SHJ, CIGS, and IMM solar cells. Hypothesis testing was conducted in an environment simulating open space (exposure to the sun-like UV in vacuum and performance testing with a solar simulator using AMO filter). The UV exposure time varied from O to up to 7,000 ESH (corresponding to more than a year in space). All the tested solar cells are considered as good candidates for space power applications. The mechanism of converting solar UV in visible-Nm light was downshifting with ~69 and ~05% PLQY for the nano-JJowder and the SCL, respectively. The improvement of UV stability (in terms of reduction of the efficiency degradation rate) by the SCL was finnly (beyond the statistical spread) observed for all three types of the cells. The degradation of the SHJ and IMM cells was reversed to zero or slight growth while the degradation of the CIGS decreased by ~ 25%. Possible mechanisms of improvement included absorption and reflection of harmful solar lN, shielding UV-sensitive front conductors (as in the case of CIGS cells), and the gradual improvement of the optical coupling over time. The positive impact of the downshifted PL on PV efficiency was shaded by the loss of the incident visible solar light due to reflection and scattering from the SCL. Possible but small, positive contribution of the downshifted PL was indirectly observed in the case of the SHJ and IMM cells. To further improve the stabilizing effect and implement the increase in PV efficiency of the coated cells, the SCL will have to be set free of large-size light scattering impurities. The layer has also to be textured and antireflection-coated to minimize reflection of the incident visible solar light

Qualitatively different behavior of each cell material visible in Figure 25 suggests that phenomenological compatibility of cell base compound and coating properties might be the most important "ingredient" of the combination; maybe each cell material has its own best coating. For instance, CORIN worked better for CIGS than SCL as a UV stabilizer but SCL was better than CORIN for SHJ and IMM. The future work will focus on the search for an optimal protective SCL coating for each type of PV cell. This will include the selection of suitable polymer base, spectrum downshifting phosphor, composition, concentration, and layer structure.

Since most space and low-orbit vehicles (such as Elon Musk's Starlink constellation) rely on solar power, the proposed polymer nanocomposite layers that increase the operational lifetime and power efficiency of the coated solar panels have a great commercial potential.

Funding information : Dillard team appreciates the financial support from US Air Force Office of Scientific Research Grant Nos FA9550-18-1-0364 and FA9550-23-1-0611 and Anny Research Office Grant No. W911NF-22-10128 and the partial support from Dillard University Minority Health and Health Disparity Research Center MHHDRC. Dr. Patel's research was sponsored by the NSF Grant No. 2200426. Drs Sarkisov, PateL and Fedoseyev also acknowledge the support from NASA amtracts Nos 80NSSC22PB171 and 80NSSC22PB198.

Author contribution s: Abdalla **M.** Darwish: conceptualization, investigation, and writing; Sergey S. Sarkisov: conceptualization, investigation, and writing ~ reviewing and editing; Brandon Graycol: investigation ; Anja Hribljan: investigation; Darayas N. Patel: conceptualization and investigation; Alex Fedoseyev: conceptualization and investigation; David Hui: conceptualization; Paolo Mele: conceptualization; Giovanna Latronico: inv estigation; Kyu Cho: conceptualization; Anit Giri: conceptualization; and Brent Koplitz: conceptualization. All authors have accepted responsibility for the entire content of this manuscript and approved its submission. The views and conclusions contained in this document are those of the authors and should not be interpreted as representing the official policies, either expressed or implied, of the U.S. Govern me nt. The U.S. Government is authorized to reproduce and distribute reprints for Government purposes notwithstanding any copyright notation herein.

Conflict of interest: David Hui, who is the co-author of this article, is a current Editorial Board member of *Nanotechnology Reviews*. This fact did not affect the peer-review process. The authors declare no other conflict of interest

References

[1] CORIN XLS Polyimide. Nexolve. 2023. https:// hybridplasticsc.com/wp-content/uploads/2015/04/CORIN.pdf.

[2] Finckenor MM, Rodman L, Farmer B. Analysis of fluorinated polyimides flown on the Materials International Space Station Experiment. NASA. 2015; NASA/TM. 2015;218205, https://ntrs.nasa.gov/api/citations/20150016168/downloads/20150016168.pdf.

[3] CPI"" Polyimide. Nexolve. 2023. https://nexolve.com/wp-contenU uploads/2021/10/TDS_CPI_Clear.pdf.
[4] Optinox® SR Films and Coatings. Nexolve. 2023. https://nexolve. com/wp-contenUuploads/2021/10/TDS_Optinox_SRpd f.
[SJ Nexolve Essar"" Stretch 255 Polyimide. Shonghan Plastic Technology Co., Ltd. 2023. http://www.lookpolymers.com/ polymer_NeXolve--Essar-Stretch-255-Polyimide.php.
[6] Carr JA, Johnson L, Boyd D, Phillips B, Finckenor M, Farmer B, et al. LISA-T part three:The design and space environments testing of a thin-film power generation and communication array. Acta Astronaut. 2023;205:267-80.
[7] Baker CC, Fontana J, KimW, Bowman SR, SangheraJ, BallatoJ, et al. Nanoparticle doping for high power fiber lasers at eye-safer wavelengths. Opt Express. 2017;25(12):3903-13915.
[8] Wang X, Zhao S, Zhang Y, Sheng G. Controlled synthesis and tun• able luminescence of NaVF4:Eu3 . J Rare Earth. 2010;28:222-4.
[9] Xie A, Liu X, Xiong Y. Eu3+ doped K--1.u-F system optical materials: controlling synthesis, phase evolution, and optical properties. J Rare Earth. 2015;33(12):1261-7.
[10] Li S, Li Y, Sun J, Man X. Synthesis and photoluminescent characteristics of Eu•3-doped MMoO 4 (M = Sr,Ba) nanophosphors by a hydrothermal method. J Rare Earth. 2017;35(4):347-55.
[11] Zoghbi ME, Altenberg GA. Membrane protein reconstitution in nanodiscs for luminescence spectroscopy studies. Nanotech Rev. 2017;6(1):33-46.
[12] Geitenbeek RG, de Wijn HW, Meijerink A. Non-Boltzmannlumi- nescence in NaYF4:Eu3•: Implications for luminescence thermo- metry. Phys Rev Appl. 2018;10:064006.
[13] Han Q, Hao A, Gao W, Qi J, Wang Y, Dong J. Luminescence mechanism of Eu3+ ions doped NaYF4 nanocrystals *via insitu* time-- resolved spectroscopy. Ceram Intern. 2020;46:11132-36.
[14] Godlewski MM, Kaszewski J, Kielbik P, Olszewski J, Lipinski W, Slonska-Zielonka A, et al. New generation of oxide-based nano- particles for the applications in early cancer detection and diag• nostics. Nanotech Rev. 2020;9:274-302.
[15] Elkodous MA, El-Husseiny HM, El-Sayyad GS, Hashem AH, Doghish AS, Elfadil D, et al. Recent advances in waste-recycled nanomaterials for biomedical applications: Waste-to-wealth. Nanotech Rev. 2021;10:1662-739.
[16] Madani M, Hosny S, Alshangiti DM, Nady N, Alkhursani AA, Alkhaldi H, et al. Green synthesis of nanoparticles for varied applications: Green renewable resources and energy-efficient synthetic routes. Nanotech Rev. 2022;11:731-59.
[17] Duan H, Wang T, Su Z, Pang H, Chen C. Recent progress and challenges in plasmonic nanomaterials. Nanotech Rev. 2022;11:846-73.
[18] Elkodous MA, HamadHA, Abdel Maksoud MIA, Ali GAM, El Abboubi M, Bedir AG, et al. Cutting-edge development in waste-- recycled nanomaterials for energy storage and conversion appli• cations. Nanotech Rev. 2022;11:2215-94.
[19] Patel D, Sarkisov S, Darwish A, Ballato J. Optical gain in capillary light guides filled with NaYF4: Yb3\ Er3• nanocolloids. Opt Express. 2016;24(18):21147.
[20) Wang Z·J, Tao F, Cai W•l, Yao L-Z, Li X-G. Hydrothermal synthesis of NaEuF4 spindle-like nanocrystals. Bull Mater Sci. 2011;34(7):1371-4.
[21] Kesavulu CR, Kumar KK, Vijaya N, Lim KS, Jayasankar CK. Thermal, vibrational and optical properties of Eu3•-doped lead fluoropho• sphate glasses for red laser applications. Mater Chem Phys. 2013;141:903-11.
[22] Zhydachevskyy Y, Tsiurma V, Baran M, Lipinska L, Sybilski P, Suchoki A. Quantum efficiency of the down-conversion process in Bi•3/- Yb•3 co-doped Gd_2O_3. J Lumin. 2018;196:169-73.
[23] Panday S. Triple-Junction Solar Cells for Space Exploration. LEDs & Solar Cell Course at UIUC. 2019. https: //443.ece.illino is.edu/files/ 2019/05/SolarCellReportPandeyWaterMarked.pdf.
[24] Li S, Pomaska M, Lambertz A, DuanW, Bittkau K, Qiu D, YaoZ, et al. Transparent-conductive--oxide--free front contacts for high-eff ciency silicon heterojunction solar cells. Joule. 2021;5:1535-47.
[25] Radha K Development of four -t erminal devicesutilising thin-film solar cells. MS thesis. Delft, Netherlands: Delft University of Technology; 2018.
[26] Poe G, Farmer B. Polyimide polymer with oligomeric silses-- quioxane. U.S. patent 7619042B2; November 2009.
[27] Poe G, Farmer B. Polymeric coating for protecting objects.U.S. patent 8053492B2; November 2011.
[28] Darwish A, Sarkisov S, Mele P. Nano<omposite thermo-electric energy converter and fabrication method thereof. U.S. patent 10283691B2; May 2019.
[29] Darwish A, Sarkisov S. Method and apparatus for open-air pulsed laser deposition. U.S. patent 10316403B2; June 2019.
[30] Darwish A, Sarkisov S. Multiple beam pulsed laser deposition of composite films. U.S. patent 11059128B2; July 2021.
[31] Darwish AM, Sagapolutele MT, Sarkisov S, Patel D, Hui D, Koplitz B. Double beam pulsed laser deposition of composite films of poly (methyl methacrylate) and rare earth fluoride upconversion phos- phors. Compos Part B - Eng. 2013;55:139-46.
[32] Darwish AM, Wilson S, Sarkisov S, Patel D. Double beam pulsed laser deposition of polymer nanocomposite NaYF4:Tm3, Yb3 films for optical sensors and light emitting applications. In: Yin S, Guo R, editors. Photonic fiber and crystal devices: advances in materials and innovations in device applications VII. Proceedings of SPIE 8847. San Diego, CA. Bellingham, WA: SPIE; 2013 Sept. p. 884702.
[33] Darwish AM, Burkett A, Blackwell A, Taylor K, Sarkisov S, Patel D, et al. Polymer-inorganic nano-composite thin film upconversion light emitters prepared by double-beam matrix assisted pulsed laser evaporation (DB-MAPLE method. Compos Part B - Eng. 2015;68:355-64.
[34] Darwish AM, Burkett A, Blackwell A, Taylor K, Walker V, Sarkisov S, et al. Efficient upconversion polymer-inorganic nanocomposite emitters prepared by the double beam matrix assisted pulsed laser evaporation (DB-MAPLE). In: Yin S, Guo R, editors. Photonic fiber and crystal devices: advances in materials and innovations in device applications VIII. Proceedings of SPIE 9200. Vol. 92000. San Diego, CA. Bellingham, WA: SPIE; 2014 Sept.
[35] Darwish AM, Wilson S, Blackwell A, Taylor K, Sarkisov SS, Patel DN, et al. Ammonia sensor based on polymer-inorganic nano-compo• site thin film upconversion light emitter prepared by double-beam pulsed laser deposition. AmJ Mater Sci. 2015;5(3A):8-15.
[36] Darwish AM, Wilson S, Blackwell A, Taylor K, Sarkisov S, Patel D, et al. Polymer-inorganic nanocomposite thin film emitters, optoe- lectronic chemical sensors, and energy harvesters produced by multiple-beam pulsed laser deposition. In: Yin S, Guo R, editors. Photonic fiber and crystal devices: advances in materials and innovations in device applications IX: Proceedings of SPIE 9586. San Diego, CA. Bellingham, WA: SPIE; 2015 Aug. p. 958602
[37] Darwish AM, Wilson S, Blackwell A, Sarkisov S, Patel D, Mele P, et al. Multi-beam pulsed laser deposition: new method of making nanocomposite coatings. In: Yin S, Guo R, editors. Photonic fiber and crystal devices: advances in materials and innovations in

device applications IX: Proceedings of SPIE 9586. San Diego, CA. Bellingham, WA: SPIE; 201S Aug. p. 95860S.

[38] Darwish AM, Moorea S, Muhammad A, Sarkisov SS, Patel DN, Mele P, et al. Organic-inorganic nano-composite films for photonic applications made by multi-beam multi-target pulsed laser deposition with remote control of the plume directions. In: Yin S, Guo R, editors. Photonic fiber and crystal devices: advances in materials and innovations in device applications X: Proceedings of SPIE 9958. San Diego, CA. Bellingham, WA: SPIE; 2016 Sep. p. 995802.

(39] Darwish AM, Moore S, Muhammad A, Sarkisov S, Patel D, Mele P, et al. Polymer nano<omposite films with inorganic upconversion phosphor and electro-optic additives made by concurrent triple-beam matrix assisted and direct pulsed laser deposition. Compos Part B - Eng. 2017;109:82-90.

(40] Darwish AM, Sarkisov SS, Patel DN. Concurrent multi-target laser ablation for making nano-composite films Chapter 6. In: Yang D, editor. Applications of laser ablation - Thin Film Deposition, Nanomaterial Synthesis and Surface Modification. Rijeka, Croatia: InTech; 2016. p. 129-48.

(41] Darwish AM, Sarkisov SS, Patel DN, Muhammad A, Thompson K, Johnson M, et al. Polymer nanocomposite luminescent films for solar energy harvesting made by concurrent multi-beam multi-target pulsed laser deposition. In: Yin S, Guo R, editors. Photonic fiber and crystal devices: advances in materials and innovations in device applications XII: Proceedings of SPIE 10755. San Diego, CA. Bellingham, WA: SPIE; 2018 Sep. p. 107552.

[42] Darwish AM, Sarkisov SS, Patel DN. Nanocomposite luminescent solar concentrators: Optics for green energy. Asian J Phys. 2018;27(9-12):625-36.

(43] Darwish AM, Sarkisov SS, Wilson J, Muhammad A, Thompson K, Patel DN, et al. Luminescent solar concentrators based on polymer nanocomposite films made by open-air pulsed laser deposition. In: Yin S, Guo R, editors. Photonic fiber and crystal devices: advances in materials and innovations in device applications XII: Proceedings of SPIE 11123. San Diego, CA. Bellingham, WA: SPIE; 2019 Sep. p. 1112302.

(441 Darwish AM, Sarkisov SS, Patel DN. Nanocomposite windows converting solar power into electricity for self-sustaining buildings. In: Bumajdad A, Bouhamra W, Alsayegh OA, Kamal HA, Alhajraf SF, editors. Gulf Conference on Sustainable Built Environment. Cham, Switzerland: Springer Nature Switzerland AG; 2020. p. 367-82.

(45] Darwish AM, Sarkisov SS, Wilson S, Collins E, Patel DN, Paolo Mele P, et al. Quantum cutting organic-inorganic nanocomposites. In: Yin S, Guo R, editors. Photonic Fiber and Crystal Devices: Advances in Materials and Innovations in Device Applications XV: Proceedings of SPIE 11826. San Diego, CA. Bellingham, WA: SPIE; 2021 August. p. 1182606.

(46] Darwish AM, Sarkisov SS, Wilson S, Wilson J, Collins E, Patel DN, et al. Polymer nanocomposite sunlight spectrum down<onverters made by open-air PLD. Nanotech Rev. 2020;9:1044-58.

(47] PVIV Series IV Station, User's Manual. Newport. 2018. https://www.newport.com/medias/sys_master/software/software/h32/he9/9132470796318/MPVIV-IV-Station.pdf.

(48] Application Note 47. The Challenge of Making Reliable Solar Cell Measurements. Newport Corporation Technology and Applications Center. 2020. https://www.astm.org/e0948-16r20.html.

(49] ASTM E948-16 Standard. https://cdn.standradsi.teh.ai/samples/106558/ee0b2a87bb964cfic9d28130386bb9c44/ASTM-E948-16-2020p.pdf.

[SO] Sinha A, Qian], Moffitt SL, Hurst K, Terwilliger K, Miller DC, et al. UV-induced degradation of high-efficiency silicon PV modules with different cell architectures. Prog Photovolt Res Appl. 2023;31:36-51.

(51] Malm U. Modelling and degradation characteristics of thin-film CIGS solar cells. Ph. D. thesis. Uppsala, Sweden: Uppsala University; 2008.

(52] Wang J. Open-circuit voltage, fill factor, and heterojunction band offset in semiconductor diode solar cells. EcoMat. 2022;4:e12263.

(53] Salhi B. The photovoltaic cell based on CIGS: Principles and technologies. Materials. 2022;15(5):1908.